Computational markers for personalized prediction of outcomes in non-small cell lung cancer patients with brain metastases

Sébastien Benzekry (sebastien.benzekry@inria.fr)
Inria Sophia Antipolis – Méditerranée, Inserm UMR1068, CNRS UMR7258, Aix Marseille University UM105

Pirmin Schlicke
Technical University of Munich

Alice Mogenet
Assistance Publique - Hôpitaux de Marseille, Aix Marseille University

Laurent Greillier
Assistance Publique - Hôpitaux de Marseille, Aix Marseille University

Pascale Tomasini
Assistance Publique - Hôpitaux de Marseille, Aix Marseille University

Eléonore Simon
Assistance Publique - Hôpitaux de Marseille, Aix Marseille University

Research Article

Keywords: Non-small cell lung cancer, Brain Metastases, Computational Biomarkers

Posted Date: September 25th, 2023

DOI: https://doi.org/10.21203/rs.3.rs-3367167/v1

Additional Declarations: No competing interests reported.

Version of Record: A version of this preprint was published at Clinical & Experimental Metastasis on December 20th, 2023. See the published version at https://doi.org/10.1007/s10585-023-10245-3.

Computational markers for personalized prediction of outcomes in non-small cell lung cancer patients with brain metastases

Sébastien Benzekry [1* †], Pirmin Schlicke [2*], Alice Mogenet [3], Laurent Greillier [3,4], Pascale Tomasini [3,4*], Eléonore Simon [3*]

1. COMPutational pharmacology and clinical Oncology Department, Inria Sophia Antipolis – Méditerranée, Cancer Research Center of Marseille, Inserm UMR1068, CNRS UMR7258, Aix Marseille University UM105, Marseille, France

2. Department of Mathematics, TUM School of Computation, Information and Technology, Technical University of Munich, Garching (Munich), Germany

3. Multidisciplinary Oncology and Therapeutic Innovations Department, Assistance Publique - Hôpitaux de Marseille, Aix Marseille University, Marseille, France.

4. Aix Marseille University, CNRS, INSERM, CRCM, Marseille, France

***** These authors contributed equally and are co-first authors in alphabetical order.

[†] Corresponding author: sebastien.benzekry@inria.fr

Faculté de Pharmacie, 27 boulevard Jean Moulin, 13005 Marseille, France

+33695725707

The authors declare no conflict of interest.

Social media handles:

Authors: @SBenzekry, @PirminSchlicke

Institutions: @aphm_actu, @crcm_marseille, @inria_sophia, @tu_muenchen

ABSTRACT

Background:

Intracranial progression after curative treatment of early-stage non-small cell lung cancer (NSCLC) occurs from 10 to 50% and is difficult to manage, given the heterogeneity of clinical presentations and the variability of treatments available. The objective of this study was to develop a mechanistic model of intracranial progression to predict survival following a first brain metastasis (BM) event.

Methods:

Data included early-stage NSCLC patients treated with a curative intent who had a BM as the first and single relapse site (N=31).

We propose a mechanistic mathematical model to estimate the amount and sizes of (visible and invisible) BMs. The two key parameters of the model are α, the proliferation rate of a single tumor cell; and μ, the per day, per cell, probability to metastasize. The predictive value of these individual computational biomarkers was evaluated.

Findings:

The model was able to correctly describe the number and size of metastases at the time of first BM relapse for 20 patients. Parameters α and μ were significantly associated with overall survival (OS) (HR 1.65 (1.07-2.53) p=0.0029 and HR 1.95 (1.31-2.91) p=0.0109, respectively). Adding the computational markers to the clinical ones significantly improved the predictive value of OS (c-index increased from 0.585 (95% CI 0.569-0.602) to 0.713 (95% CI 0.700-0.726), p<0.0001).

Interpretation:

We demonstrated that our model was applicable to brain oligoprogressive patients in NSCLC and that the resulting computational markers had predictive potential. This may help lung cancer physicians to guide and personalize the management of NSCLC patients with intracranial oligoprogression.

Highlights:

- Mechanistic mathematical modeling allows individualized prognosis of survival for lung cancer patients after first brain metastatic relapse

- Individual model-derived computational parameters identifies high-risk patients in terms of brain metastasis progression and survival

- Prognostic features include quantification of the number and sizes of both clinically visible and invisible brain metastases

Classification: Biological Sciences, Applied Mathematics

Keywords: Non-small cell lung cancer, Brain Metastases, Computational Biomarkers

Statements and declarations

Non-small cell lung cancer is difficult to manage when brain metastases are present. This study presents a mathematical model that can be calibrated on individual patients' data early in the treatment course to explain the growth dynamics of brain metastases and demonstrates that the mathematically derived parameters can serve as predictive tool in clinical routine care.

Conflict of Interest / Disclosure

Competing interests

None of the authors reports interests related to the present work.

Funding

None

INTRODUCTION

The 5 years survival rate of non-small cell lung cancer (NSCLC) patients is only 17%[1,2]. This poor prognosis is partly due to the frequency of brain metastases (BM), occurring in up to 50% of NSCLC patients[3] and directly responsible for death in 50% cases[4,5]. Even in initially early-stage NSCLC treated with curative intent, intracranial relapse occurs in 10% of the cases in stage I-II NSCLC and 30 to 50% cases in stage III NSCLC[6]. Not only is the brain one of the first sites of recurrence after surgery or curative radiotherapy, but it can also be the only site of relapse, then called intracranial oligoprogression[7–9].

Oligoprogression is defined as the progression of a limited number of metastases, ranging from 3 to 5, and possibly treated by local therapies[10–12] . Existing data on intracranial oligoprogression are mostly related to palliative situations, and to patients receiving tyrosine kinase inhibitors[13]. There are no real guidelines for the management of single intracranial oligoprogression in patients with early-stage NSCLC at diagnosis, initially treated with curative intent. Furthermore, the difficulty in establishing guidelines relies on the heterogeneity of this situation. Some patients undergo a single intracranial recurrence, while others suffer from either multiple intracranial relapse or subsequent extra-cranial relapse[14].

Several options are available for the treatment of BM, including local and systemic therapies. Local treatments include neurosurgery, stereotaxic radiosurgery (SRS) and whole brain radiotherapy (WBRT)[15–19]. Local treatment indications have evolved over time and the place of SRS is becoming increasingly important[16–20]. Nevertheless, WBRT has the advantage of covering all macroscopic and microscopic BMs which would not be detected with MRI and could have a prophylactic role on the development of BM[21,22]. However, WBRT is also responsible for neurocognitive decline, leading to a lower quality of life[23,24].

On the other hand, systemic treatments include chemotherapy, targeted therapies or immunotherapy[10,25–28]. The intracranial efficacy of systemic treatments is heterogeneous and partly depends on drugs potential to cross the blood-brain barrier (BBB) [29]. Moreover, the unique brain microenvironment likely plays a critical role in treatment response, especially with immunotherapy[30–33]. The combination of systemic treatments such as chemotherapy and immunotherapy seems to induce better intracranial response than immunotherapy alone[34,35]. Combinations of local and systemic treatments also seem to have a synergistic effect and lead to better intracranial response[36]. Radiotherapy (either SRS or WBRT) could help damage the BBB, allowing the crossing of systemic treatments.

The complexity of multimodal management of BM relies on the diversity of possible treatments (including local and systemic treatments), the difficulty of crossing the BBB for systemic treatments, the specificity of the brain microenvironment and the lack of predictability of the appearance of BM, as well as further extracranial progression, as evidenced by Levy's study of European practices[37]. To guide the management of patients with BM, prognostic scores have been established, such as the mol-Lung GPA[38–40]. However, these scores do not help predict the occurrence of metastases, even if some predictive factors were identified such as age ≤ 62, stage T4 or N2-3, adenocarcinoma subtype, the presence of leukoaraiosis, and molecular profile[41,42].

Predicting the course and the appearance of BM would improve the monitoring of patients and offer a more personalized treatment. For this purpose, the contribution of mathematical modeling can be crucial. The first mathematical models of metastatic occurrence based on experimental observations were established by Liotta in the 1970's[43]. Further mathematical models were then established in animal models[44–46]. These models were based on two main phenomena: growth and spread of a tumor. The latter is often successfully described using the Gompertz model[47–49]. For metastatic spread, we have developed models based on pioneering work by Iwata et al[45,46,50,51]. Our team further developed these mathematical models to be applicable in the clinic, for example on breast[52] or kidney[53] cancer. This model was then developed within the framework of NSCLC BMs[54]. This last work proposed a method to determine the age of the disease according to the pathology and size of the primary tumor, to test different dissemination and colonization scenarios and finally to predict the appearance and growth of BMs over time. However, this preliminary work only included two patients and was addressing a proof-of-concept for description of BM history. The interest of this new study is to validate the mathematical model on a larger cohort of patients and to apply it to the specific situation of intracranial oligoprogression.

The primary objective of this study was to develop the mathematical model and apply it to a situation of intracranial oligoprogression in patients with early-stage NSCLC, initially treated with a curative intent. The secondary objective was to assess the association of the outcomes predicted with this model with overall survival and progression-free survival.

MATERIALS & METHODS

Data. We retrospectively investigated all early-stage NSCLC patients treated with a curative intent who had intracranial oligoprogression treated at *Assistance Publique Hôpitaux de Marseille* (APHM) in the department of Multidisciplinary Oncology and Therapeutic Innovations. We enrolled all patients with BM as the first site of relapse. Patients with primary tumor progression or metastatic extracranial progression at the time of brain oligo-progression were excluded. Patients with ongoing systemic treatment at the time of oligo-progression were also excluded. This study was approved by the institution review board (IRB # 2021-25).

Patients' characteristics (including sex, age, smoking history, performance status), NSCLC data (pathology, stage at diagnosis, molecular profile), treatment data (treatment received for the primary tumor, history of BM treatment) and outcome data (size and number of BM at first relapse, longitudinal data of BM, progression-free survival (PFS) and overall survival (OS)) were investigated. OS was defined as the time from diagnosis of the primary tumor to death from any cause (or date of last follow up). PFS was defined as the time between the first metastatic relapse and second progression or death from any cause (or date of last follow up).

Since the model presented in this study was based on numbers of cells, the longitudinal diameter measurements of the data set were converted by assuming spherical shape. These volumetric data were then rescaled into cell numbers using the conversion rule $1\text{mm}^3 = 10^6$ cells[55].

Model definition. Primary tumors were assumed to follow Gompertzian growth[56,57]. The initial size of a tumor at time $t = 0$ was assumed to be of exactly one cell, i.e., $S_P(0) = 1$[58]. The parameter α_P can be interpreted as the initial specific growth rate of a single tumor cell and the parameter β_P is the exponential decay factor of this specific growth rate[59]. The analytical solution of the growth dynamics for the primary tumor and the analogous dynamics for the metastases are given in the supplementary material with α the initial specific growth rate of a metastatic cell and β its corresponding decay factor analogous to the definitions above.

Two additional parameters μ and γ were introduced for the dissemination process: μ stands for the probability per day and per cell for a tumor cell to succeed going through all steps of the postulated metastatic cascade[60]. Parameter $\gamma \in [0,1]$ describes how the geometrical structure of the tumor enables the tumor to seed new metastases.

The model equations for the number of metastases (visible and invisible) are described in the supplementary material and details to this approach were previously published[60]. Since there is evidence that secondary and thus lately seeded metastases are of minor clinical relevance[61], for the purpose of our predictive framework we focused on metastases seeded by the primary tumor only. The model was implemented in Matlab.

Parameter assumptions. Following Bilous et al.[60] we reduced further the number of free parameters to ensure practical identifiability. We assumed a maximum carrying capacity of $exp(\alpha/\beta) = 10^{12}$ cells[62] for both the primary tumor and metastases' growth kinetics. Since longitudinal pre-diagnosis measurements of primary tumors were not available, we assumed a pathology-dependent doubling time estimated from a previous meta-analysis[60]. Specifically, doubling times were assumed to be 201, 104 and 91 days for adenocarcinoma, squamous cell carcinoma and undifferentiated carcinoma, respectively[60]. The metastases observed clinically, i.e., the visible BMs, are assumed to be larger than the volume s_v corresponding to a diameter measurement of three mm.

Parameter identification. The procedure to determine the size and number of BMs from the model equations and values of the parameters is described in the supplementary material. The doubling time of a primary tumor at the time of primary diagnosis was used to determine the two growth parameters α_P and β_P (see supplementary material). Preliminary exploration of the parameter space suggested that a value of $\gamma = 0.1$ was able to describe the data. Only parameters α and μ were considered specific to each patient and identified from fitting the model to the data performed using GlobalSearch[63,64] (see supplementary material for details).

Statistical analysis. These two computational parameters α and μ were used as computational biomarkers with potential additional prognosis value. We analyzed the association of these parameters with OS and PFS using a previously published method[65]. Log-rank statistical tests were performed on dichotomized groups (with threshold taken at the median value of the computational biomarker)[66]. In addition, multivariable proportional hazard Cox regression models were considered, either using only the clinical covariates or the clinical covariates augmented with α and μ. These were implemented using the *lifelines* python package[67]. The predictive ability of these Cox models

was determined calculating the mean value of Harrell's c-index[68] of one hundred replications of a three-fold cross-validation procedure. In a closer examination, only covariates below a significance level $p < 0.2$ were selected for multivariable analysis. To determine the statistical significance of mean c-indices between Cox models, two-sample t-tests were conducted.

RESULTS

Data presentation and description

We identified 31 patients who had intracranial oligoprogression after initial treatment with a curative intent for early-stage NSCLC. Of these, 10 were women and 21 were men. There were 9 squamous cell carcinomas and 22 non-squamous carcinomas, including 20 adenocarcinomas. At the time of diagnosis, 20 patients were stage I/II and 11 were stage III according to the 8th TNM classification. Number of BMs lied between one and three and the corresponding diameter sizes between 4 mm and 75 mm. Treatment received for the primary tumor and the number and treatment of brain metastasis at the first relapse are reported in Table 1. 17 patients had more than one intracranial recurrence. Median OS was 80.98 months (95% CI 37.56 – 98.27) and median PFS was 11.73 months (95% CI 4.93 – 27.20).

The data included values of longitudinal diameter measurements determined via computed tomography (CT) and magnetic resonance imaging (MRI) images of primary tumors and BMs as well as the time of relapse and time of death. Representative patient plots of these time series data are reported in Figure 1.

Out of the 31 patients, three patients had no primary tumor measurements at primary diagnosis. In the later analysis, these patients had to be excluded, since the primary tumor growth parameter calibration could not be performed (cf. Mathematical model).

Table 1. Data description: Patient overview. *PT = Primary tumor, BM = Brain metastases, SRS = stereotaxic radiosurgery, WBRT = whole brain radiotherapy*

Data population	**Population N 31 (%)**
Sex	
Female – Male	10 (32.3%) – 21 (67.7%)
Median Age at Diagnostic	61 (39-82)
Smoking Status	
Smoker	11 (35.5%)
Former smoker	13 (41.9%)
No smoker	1 (3.2%)
Stage at diagnostic	
I/II	20 (65%)
III	11 (35%)
Primary tumor pathology subtype	
Non squamous cell carcinoma	22 (71%)
Squamous cell carcinoma	9 (29%)
Molecular Status of PT	
EGFR	3
KRAS	4
PTEN	1
TP53	2
STK11	1
CTNNB1	1
No mutation	8
Unknown	14
Size of PT at diagnosis (diameter value)	

≤ 25 mm	14 (45%)
> 25, ≤ 50 mm	6 (19%)
> 50, ≤ 75 mm	7 (23%)
> 75 mm	1 (3%)
Unknown	3 (10%)
Surgery of the primary tumor	
Yes	22 (71%)
No	9 (29%)
Systemic treatment for the primary tumor	
Yes	19 (61.3%)
No	12 (38.7%)
Median time between the diagnosis and first relapse (months)	13.63 (95% CI 9.03 – 18.00)
Number of BM at first relapse	
1	18 (58.1%)
2	5 (16.1%)
3	8 (25.8%)
Sum of BM diameters at relapse	
≤ 20 mm	18 (58%)
> 20, ≤ 40 mm	9 (29%)
> 40 , ≤ 60 mm	3 (10%)
> 60 mm	1 (3%)
Individual BM diameters at relapse	
≤ 10 mm	25 (49%)
> 10, ≤ 20 mm	12 (24%)
> 20 , ≤ 30 mm	6 (12%)
> 30 mm	8 (16%)
Type of local treatment at first cerebral relapse	
Surgery alone	3 (9.7%)
Surgery + WBRT	4 (12.9%)
Surgery + SRS	7 (22.6%)
SRS alone	16 (51.6%)
WBRT alone	1 (3.2%)
Systemic treatment at first cerebral relapse	
Yes	11 (35.5%)
No	20 (64.5%)
Number of cerebral relapse	
1	14 (45.2%)
2-3	13 (42%)
>3	4 (12.8%)
Median time between the first and second relapse (months)	11.73 (95% CI 4.93 – 27.20)

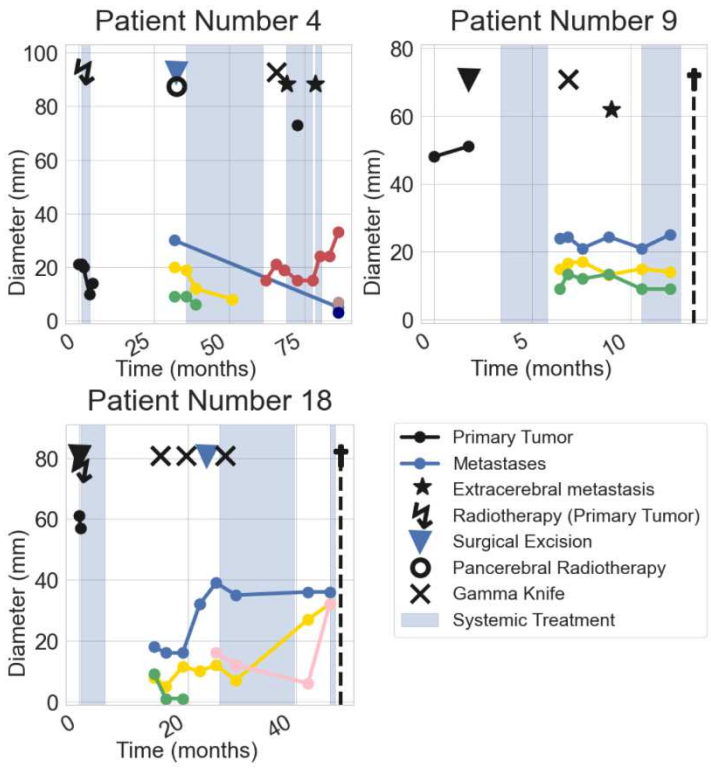

Figure 1. Patients' time course. *Time course of three example patients. Black bullets show the primary tumor size and colored bullets the brain metastases sizes. The time course was shifted such as time zero corresponds to the day of primary diagnosis. Also shown are local and systemic treatments (triangle, cross, flash, circle, colored background), the presence of extracranial metastases (black asterisk, not linked to diameter axis) and the time of death (black cross with dashed line).*

Parameter values

As explained above, the remaining parameters subject to identification through data fitting were α (growth) and μ (dissemination). Parameter values are shown in Table 2.

Table 2. Parameter description. *Population characteristics of the identified mathematical parameters α and μ and derived clinical estimations of tumor volume doubling time $\tau_{BM}(s_v)$ of the BMs at size s_v, as well as the yearly dissemination rate $\mu s_v{}^{\gamma}$ of new metastases by the primary tumor of size s_v, std = standard deviation. Recall that s_v is the volume size of a tumor corresponding to a diameter measurement of three mm.*

parameter	unit	mean	median	std	min	max
α	$[\mathrm{d}^{-1}]$	$4.93 \cdot 10^{-2}$	$4.03 \cdot 10^{-2}$	$3.18 \cdot 10^{-2}$	$1.22 \cdot 10^{-2}$	$1.34 \cdot 10^{-1}$
μ	$[\mathrm{d}^{-1} cell^{-1}]$	$3.57 \cdot 10^{-4}$	$2.33 \cdot 10^{-4}$	$2.77 \cdot 10^{-4}$	$8.22 \cdot 10^{-5}$	$1.22 \cdot 10^{-3}$
$\tau_{BM}(s_v)$	[d]	66.42	55.41	42.71	16	180
$\mu s_v{}^{\gamma}$	$[y^{-1}]$	0.83	0.54	0.65	0.19	2.85

Simulations and outcome

The model was used to simulate the history of all BMs, including those not yet clinically detectable at the time of first BM occurrence. To ensure parameter identifiability, a specific method was introduced (cf. Methods). The total number of model-predicted BM existence (clinically visible + invisible) at the time of first BM occurrence was compared to the number of BMs detected throughout the full clinical history of the individual patient and featured in the data set (Figure 2).

The BM history individual simulation for a representative patient is shown in Figure 3. Analogous simulations for all patients are shown in the supplementary material. Figure 3A shows the data of the clinical history. Panels 3B and 3C compare the model-predicted metastatic distributions at the two time points of primary diagnosis and first BM occurrence T_{BM}, respectively. The whole-time course of primary tumor and BM metastases sizes is presented in Figure 3D. The simulated visible metastases in comparison to the clinically detected metastases at time T_{BM} as well as the size distributions of BMs at the time of first BM occurrence T_{BM} are presented in Figure 3E.

Compared to the data, the model calculations produced reasonable estimations of size and number of visible BMs at the time of first BM occurrence throughout the data set. For 20 patients, the calculated theoretical number of BMs at the time of first BM occurrence was greater or equal to the number of BMs observed during the full clinical treatment of the respective patient. We considered this not only as a reasonable estimate but also a good indication that the model-predicted total number and size of BMs proves to be useful in estimating the invisible BMs early in the treatment course.

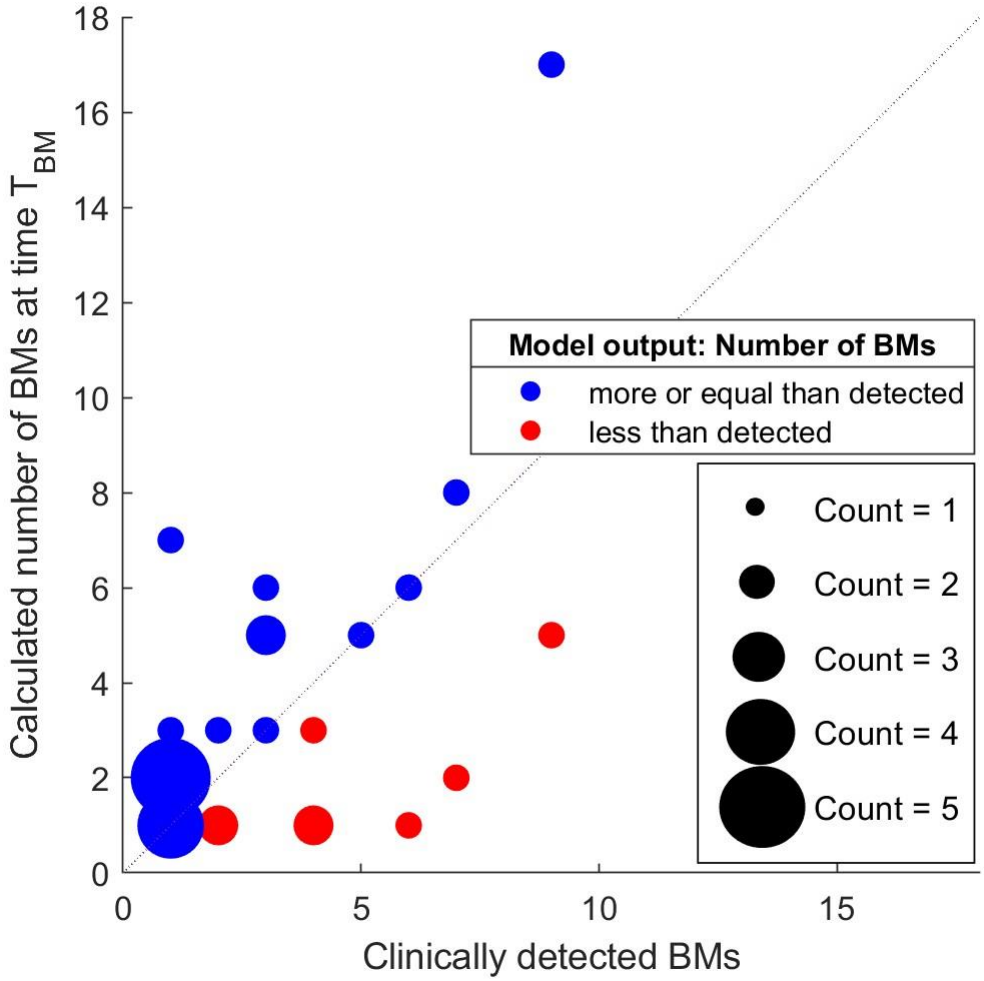

Figure 2. Model-predicted calculated total number of BMs (visible + invisible) compared to the clinically detected BMs over the treatment course. *Estimations that prognosed less (more) BMs than the number of BMs observed during the whole patients' treatment are indicated with red (blue) circles. The circles' diameters are adjusted for the respective appearance counts and are depicted in black circles in the lower right box.*

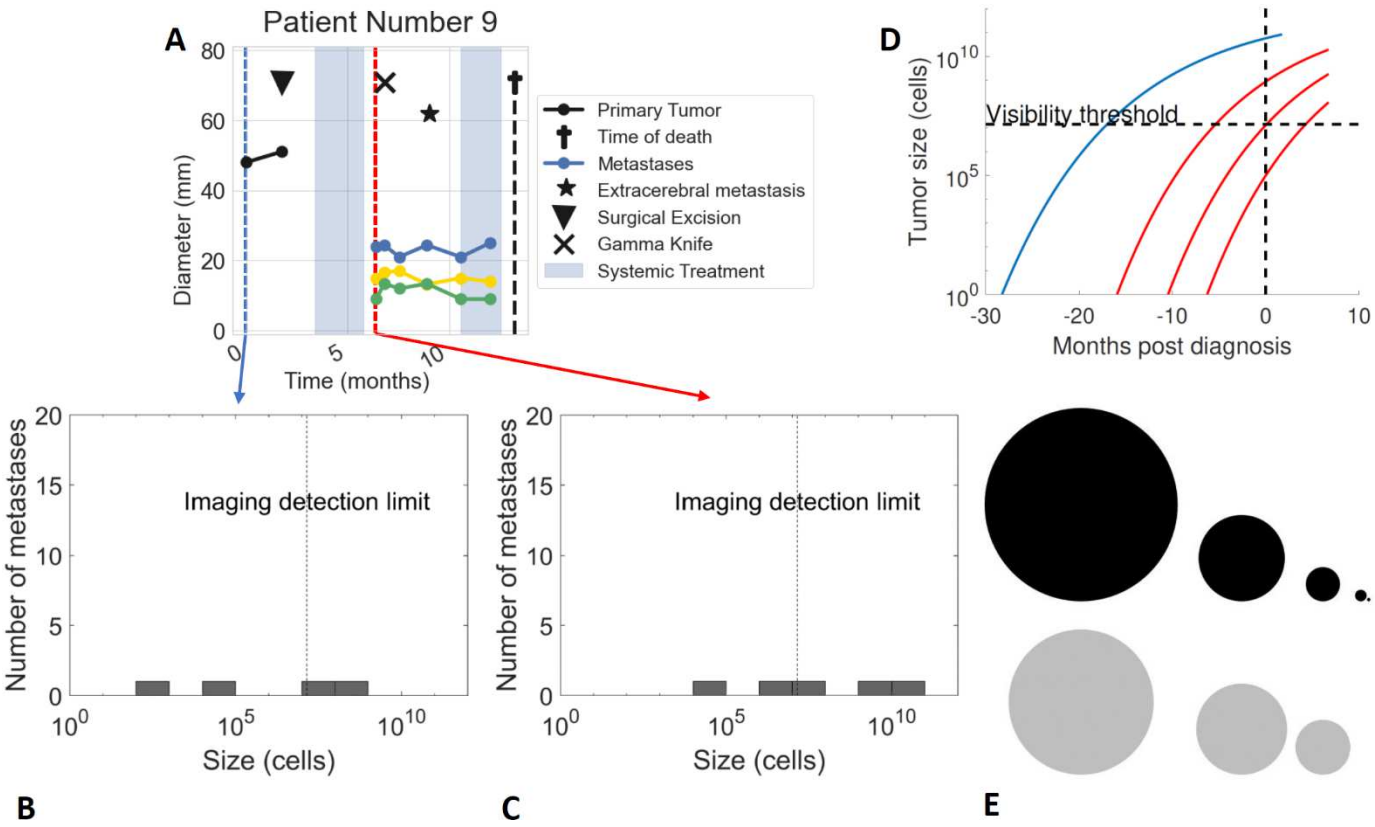

Figure 3. Simulation of one example patient. A. Clinical History. *Time series data of an example patient describes their clinical history. Data time points used for estimation of the deterministic model parameters are the primary diagnosis (blue dashed line) and the time of first BM occurrence (red dashed line). The size of the primary tumor at primary diagnosis determines the growth parameters for the primary tumor growth dynamics (cf. text). From the number and size of metastases at first BM occurrence, the two free model parameters were fitted.* ***B.*** *Model calculation allows to compute the metastatic distribution over time for the primary diagnosis.* ***C.*** *Further calculation shows the metastatic distribution at the time of first BM occurrence. Visible metastases are the ones to the right of the imaging detection limit (gray dotted line).* ***D.*** *Growth dynamics can be followed for the primary tumor (blue solid line) and the metastases (red solid line) respectively.* ***E.*** *Comparison of the computed BMs sizes at the time of first BM occurrence (black) with the observed data (gray).*

We then compared two patients with the same number of metastases at the time of first BM occurrence and relatively familiar time frames. Interestingly, the model yielded very different profiles for the invisible BMs and therefore might suggest different treatment approaches for the two patients (Figure 4).

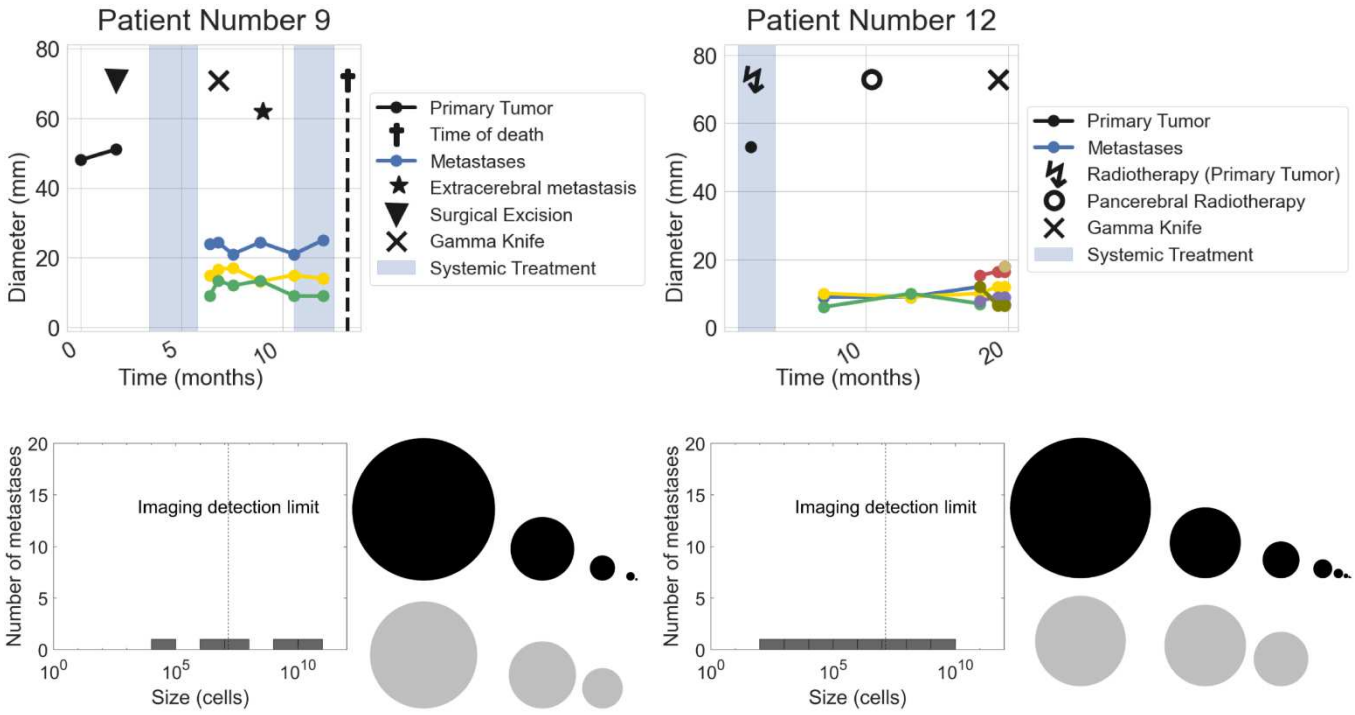

Figure 4. Comparison of two patients. *The upper row shows the full clinical history of the two patients. The estimation of the metastatic distribution at time of first metastatic relapse and the spherical representations of the corresponding metastases' sizes (black) are shown in the lower row for the respective patient, compared to the data of clinically detectable metastases (gray).*

Statistical evaluation and prediction models

To assess the predictive power of the computational markers α and μ, dichotomized Kaplan-Meier were generated for OS and PFS (Figure 5). For α, significant differences were observed for OS ($p = 0.0026$) and PFS ($p = 0.0108$). For μ, a significant difference was found at the 80% quantile for OS ($p = 0.0356$) and PFS ($p = 0.0254$), thus identifying a fraction of high-risk patients. We further assessed the association with outcome of α and μ, as well as the clinical variables in univariate Cox models (Table 3). Here, we found statistically significant hazard ratios for both the computationally determined markers α and μ for OS ($p = 0.0229$ and $p = 0.0011$, respectively).

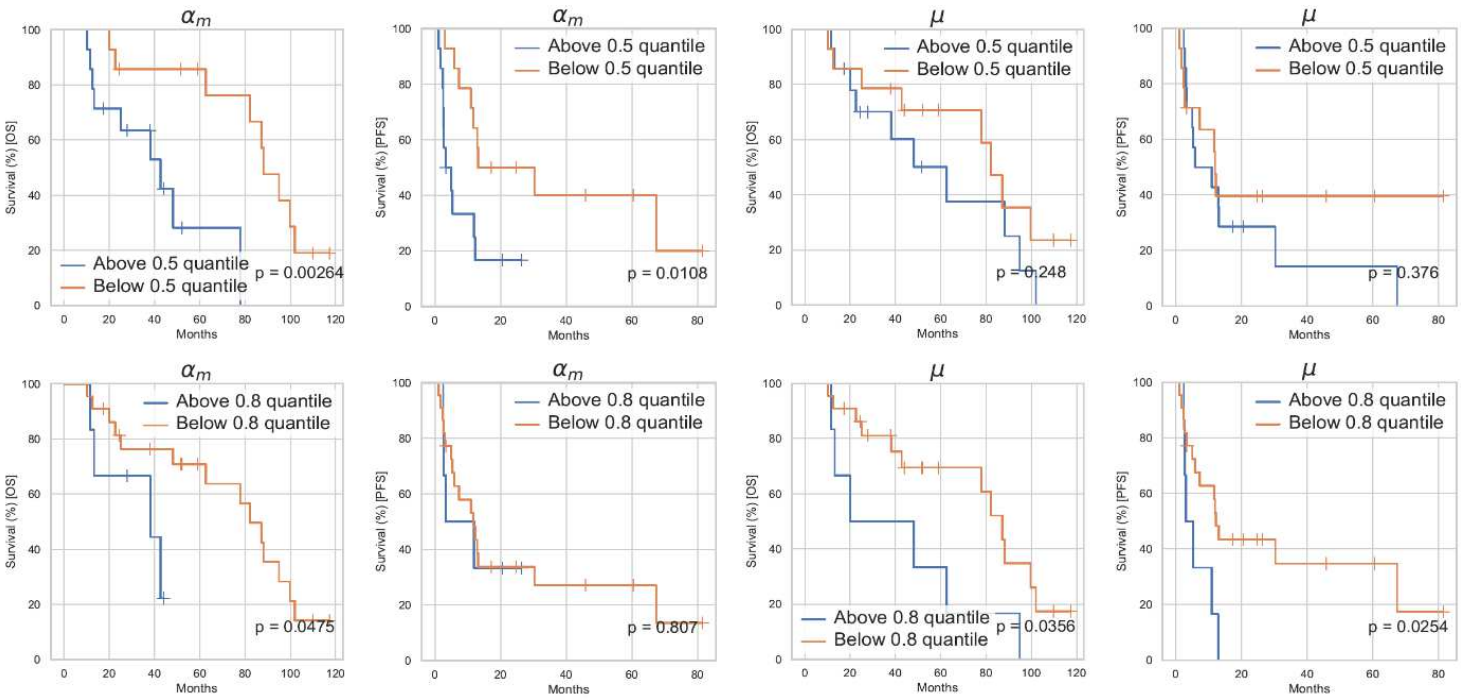

Figure 5. Kaplan-Meier curves for the computational parameters α and μ. *The survival curves for the two computational parameter groups above and below the population's median value (first row) and the 80% quantile value (second row) with respect to overall survival (first and third column) and progression-free survival (second and fourth column). The corresponding calculated p-value from the log-rank test for dichotomized groups is shown in the right lower corner.*

To determine the added value of the computational markers in comparison to the clinical data, we tested their significance in multivariable Cox models built on the clinical data alone or the clinical data and the computational markers (Figure 6 and Table 4).

Table 3: Results of the univariate Cox regression for OS and PFS. *The table shows the characteristics of the results of the univariate Cox regression including clinical and computational covariates for overall survival and progression-free survival. HR = hazard ratio, CI = confidence interval, BM = brain metastases, PT = primary tumor.*

Covariate	Hazard Ratio (OS)	p-value (OS)	95% CI (OS)	Hazard Ratio (PFS)	p-value (PFS)	95% CI (PFS)
Sex	1.1	0.602	0.768 - 1.58	0.984	0.936	0.663 - 1.46
Age at diagnosis	1.03	0.900	0.679 - 1.55	0.738	0.167	0.479 - 1.14
Number of bm at relapse	1.72	0.00556	1.17 - 2.53	1.25	0.255	0.851 - 1.84
Stage at diagnosis	0.866	0.435	0.604 - 1.24	1.1	0.674	0.716 - 1.67
Histology of pt	0.792	0.223	0.545 - 1.15	0.715	0.117	0.47 - 1.09
Parameter α	1.65	0.0229	1.07 - 2.53	1.25	0.237	0.862 - 1.83
Parameter μ	1.95	0.00109	1.31 - 2.91	1.54	0.0729	0.961 – 2.46
Size of PT at diagnosis	1.05	0.781	0.755 - 1.45	0.9	0.648	0.574 - 1.41
Size of BM at relapse	0.992	0.967	0.677 - 1.45	1.52	0.0396	1.02 - 2.26
Whole-brain radiotherapy after T_{BM}	0.89	0.539	0.615 – 1.29	0.649	0.0282	0.442 – 0.955
Systemic treatment after T_{BM}	1.16	0.420	0.807 – 1.67	0.824	0.359	0.546 – 1.25

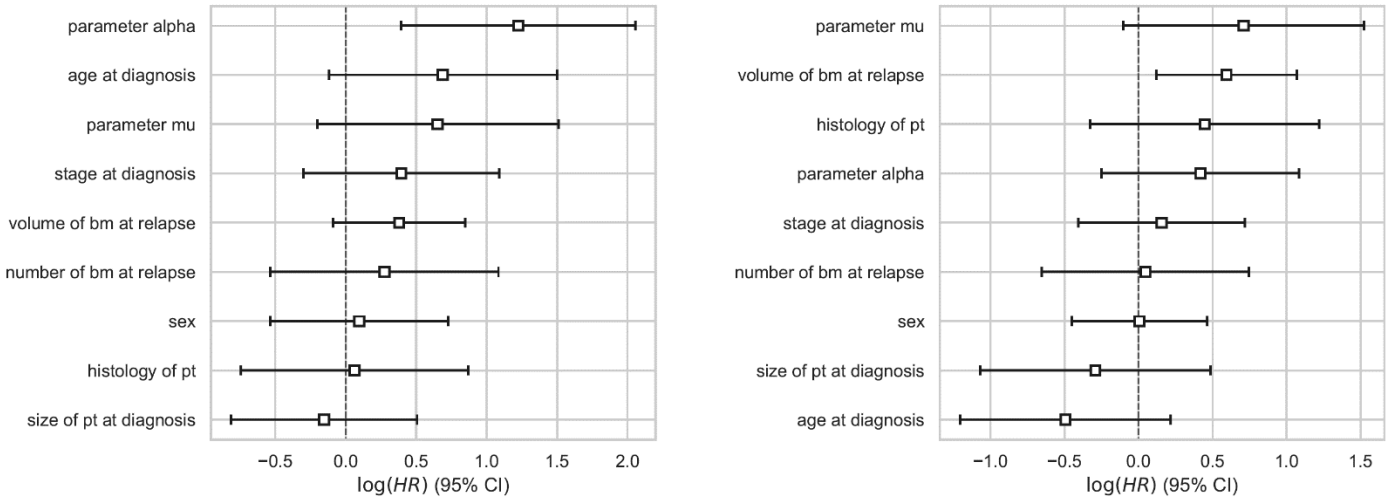

Figure 6. Hazard ratios for the predictive models. *The hazard ratios were determined performing a multivariable Cox regression. The ratios are corresponding to the predictive models for OS (left) and PFS (right) with clinical and computational covariates, i.e., the settings where the determined parameters have been added to the respective patient data.*

Table 4. Results of the multivariate Cox regression for OS and PFS. *The table shows the characteristics of the results of the multivariate Cox regression for the predictive model including clinical and computational covariates for overall survival and progression-free survival. HR = hazard ratio, CI = confidence interval, BM = brain metastases, PT = primary tumor.*

Covariate	Hazard Ratio (OS)	p-value (OS)	95% CI (OS)	Hazard Ratio (PFS)	p-value (PFS)	95% CI (PFS)
Sex	1.1	0.769	0.584 - 2.07	1.01	0.979	0.637 - 1.59
Age at diagnosis	1.99	0.0951	0.887 - 4.47	0.61	0.174	0.3 - 1.24
Number of bm at relapse	1.32	0.506	0.586 - 2.96	1.05	0.894	0.52 - 2.11
Stage at diagnosis	1.48	0.266	0.74 - 2.97	1.17	0.585	0.667 - 2.05
Histology of pt	1.06	0.879	0.475 - 2.39	1.56	0.258	0.721 - 3.39
Parameter α	3.4	0.00387	1.48 - 7.81	1.52	0.219	0.78 - 2.96
Parameter μ	1.92	0.136	0.815 - 4.52	2.04	0.087	0.902 - 4.59
Size of PT at diagnosis	0.857	0.647	0.443 - 1.66	0.748	0.463	0.344 - 1.63
Size of BM at relapse	1.46	0.113	0.914 - 2.34	1.81	0.0143	1.13 - 2.91

For OS, the c-index for those two cases were 0.585 (95% CI 0.569 to 0.602) and 0.713 (95% CI 0.700 to 0.726), respectively (statistically significant increase, p<0.0001). This drastic increase of predictive value also held in reduced models containing only variables with $p < 0.2$ in the multivariate analysis (0.647 (95% CI 0.631 to 0.664) versus 0.789 (95% CI 0.779 to 0.800), statistically significant increase, p<0.0001). For PFS, the c-indices were 0.560 (95% CI 0.545 to 0.575) and 0.595 (95% CI 0.582 to 0.608), respectively (statistically significant increase, p<0.001). Considering again only variables with $p < 0.2$ in the multivariate regression yielded c-indices of 0.708 (95% CI 0.697 to 0.718) versus 0.703 (95% CI 0.693 to 0.713).

Interestingly in both cases for OS and PFS, the prediction model with clinical variables identifies the number of visible brain metastases as variable with large hazard ratio, but the prediction model with the computational markers selects μ as having better predictive power. That is, the number of brain metastases at first metastatic relapse loses significance when the prediction model is augmented with μ. For OS, the other selected covariates besides μ were α, the age at diagnosis and the summed volume of BMs at first metastatic relapse. For the PFS, these were the age at diagnosis and the summed volume of BMs at first metastatic relapse for PFS.

DISCUSSION

Because of their prevalence and high morbidity, the management of BMs is a major issue in NSCLC. Given the heterogeneity of clinical cases and variability of treatments available, therapeutic decisions following intracranial oligoprogression are complex. Predicting the onset and evolution of BMs in NSCLC patients using mathematical modeling would offer decision support with a personalized follow-up and treatment. The objective of this study was to test a mathematical model previously developed and to apply this model to a situation of intracranial oligoprogression in patients with early-stage NSCLC initially treated with a curative intent in order to predict the outcomes and risk of recurrence of BMs after the first BM occurrence.

The clinical data collected confirmed the lack of consensus on the management of cerebral oligoprogression. At the first relapse, about 16% of patients had a WBRT that could cover brain metastases not detectable on MRI. In addition, 1/3 of patients had a systemic treatment that could optimize both intracerebral and extracerebral management.

Moreover, multiple recurrences are not uncommon, since more than 50% of patients had at least two recurrences and 12.8% had more than three recurrences in our study. The difference between OS and PFS also supports the fact that multiple recurrences will be a key element in disease control. There is also a large variability in time between two recurrences (4,93-27,2 months), which can complicate patient follow-up.

Finally, in more than 50% of cases, the diameter of the BM was less than 10mm. When we know that the threshold for BM detection is 5mm for CT scan and 1-3mm for MRI, we assume that there is a significant proportion of false negatives in the follow-up of patients in routine and which is probably why the model overestimated the number of brain metastases detected. [69,70]

These clinical data thus confirm the variability of management as well as the variability of clinical presentations in terms of number, size and recurrence of brain metastases.

We first demonstrated that the mathematical model was suitable to describe clinical history of size and number of BMs in most patients. Simulations were in lign with the data for 20 patients, while in eight cases the model underestimated the total number of BMs. However, among these eight cases the simulations correctly identified the presence of multiple BMs, which is the main point conditioning treatment decision. Among the 8 patients, there were 3 squamous cell carcinomas and 5 adenocarcinomas, 3 of which had a mutation of interest: *KRAS G12C, STK11, BRAF*. These mutations may lead to a different growth of the primary tumor or a different metastatic dissemination. BRAF and STK11 have been described as genes involved in the metastatic process[71,72]. Moreover, one of the squamous cell carcinoma had a PTEN mutation, which has been shown to be associated with BM in breast cancer[73]. Epidermoid histology and molecular biology possibly misled the model.

Furthermore, when comparing two patients with same number of BMs at the first occurrence of BM, the model was able to predict distinct evolutions that actually took place, thus guiding us in the therapeutic management.

In addition, predictive models of OS including the computational markers α and μ strongly outperformed models based on clinical variables only. For the metastatic growth rate α, significant differences were observed for OS and PFS. For the metastatic seeding μ, a significant difference was found at the 80% quantile for OS and PFS, thus identifying a fraction of high-risk patients.

Identification of a group of high risk of recurrence could assist lung cancer physicians in treatment decision.

In univariate analysis, WBRT at first BM occurrence had a significant effect on PFS (HR 0.649 (95% CI 0.442 - 0.955), p=0.0282) and systemic treatment at first BM occurrence had a minor non-significant effect (HR 0.824 (95% CI 0.546 – 1.25), p=0.359). This could be due to undetected brain metastases at the time of first BM occurrence or dormant metastatic cells. Systemic treatment or WBRT may therefore be of value for patients at risk. Indeed, WBRT has the advantage of covering all macroscopic and microscopic BM to control intracranial progression. However, WBRT does not increase survival[21,22] and leads to neurocognitive decline[23,24]. The effect of systemic treatments seems less obvious given their variable intracranial efficacy. Our model could lead to a computational tool that could assist lung cancer physicians in identifying patients with high-risk of multiple recurrences who could benefit from systemic treatments.

Furthermore, the number of metastases at recurrence was significantly associated with OS in the univariate analysis but not in the multivariate analysis. It can be assumed that a portion of BMs were undetected given the limitation of imaging. Thus, the alpha parameter brings us more significant information than the number of BM.

Other tools exist to help the management of NSCLC patients. Some are based on molecular biology prognostic scores such as the Lung-Mol GPA Score[40], others rely on radiomics features[74–77] . For example, Huang et al. demonstrated that radiomics features extracted from pre-treatment T1 MRI was an independent prognostic factor of local control for BM patients who underwent gamma knife radiosurgery[76]. The advantage of our mathematical model compared to these tools is that it is of biologically grounded and mechanistic nature. In turn, this allows to perform simulations of the disease and clinical course combined with predictive power, unlike the prognostic tools mentioned above.

The main limitation of our study is the number of patients included. It will be necessary to confirm our findings on a larger number of patients and to include molecular profiling data. However, this study was a proof-of-concept and succeeded in demonstrating the feasibility of the application of the mathematical model to a situation of NSCLC patients with BM oligoprogression.

On the other hand, the population chosen in this study (patients with early-stage NSCLC initially treated with a curative intent and presenting with intracranial oligoprogression) limits the application of our results. However, this made it possible to limit bias of systemic treatments and in this situation, lung cancer physicians are facing an unmet need with no existing guidelines.

The modeling approach remains a simplified description of the complexity of the metastatic cascade that is yet incompletely understood[78]. However, considering the limited data available, the model complexity had to be reduced to ensure practical identifiability of the parameters. This resulted in only two critical free parameters controlling growth (α) and dissemination (μ). An assumption that leaves for improvement is that primary tumor growth parameters were determined from meta-analyses values using only the tumor pathology[60]. We need further investigations to understand the influence of molecular biology, especially *EGFR* mutations[79,80] or *ALK* rearrangements because these patients have more multiple brain recurrences but have better prognosis[81]. Moreover we need to understand the impact of treatments on the primary tumor, particularly with the advent of neoadjuvant and adjuvant treatments, which could reduce micrometastatic disease and thus the risk of relapse[82–84].Moreover, our model could be extended to account for more complex processes of the metastatic cascade, such as dormancy[85] and the possibility that the primary tumor is not the only one that can spread new lesions[86] . Regarding the relapse site, we must understand the influence of the blood-brain barrier and the unique brain microenvironment[87].

However, simplifying the metastatic cascade increases the feasibility of the use of this model in clinical practice. Once the model is validated on a larger scale, applications will be developed for the clinicians to determine the risk of intracranial recurrence for each patient by selecting a few clinical parameters available in routine.

To our knowledge, this is the first mechanistic modeling approach to predict the outcomes and recurrence of BMs in NSCLC with data routinely acquired in the clinics. This work could allow to identify patients at high risk of recurrence and to propose a personalized treatment such as follow-up imaging schedule, addition of systemic or non-systemic therapy, and use of WBRT depending on the patient's risk of multiple recurrences.

ACKNOWLEDGEMENTS

PS wants to thank Christina Kuttler for valuable discussions on the mathematical modelling method. Supported by Deutsche Forschungsgemeinschaft (DFG) through TUM International Graduate School of Science and Engineering (IGSSE), GSC 81.

CONTRIBUTIONS

Conceived the research idea: SB, PT. Model setup: PS, SB. Collected the data: ES, PT. Performed data analysis and presentation: PS. Wrote software to estimate parameters and simulate: PS, SB. The paper was written by ES and PS with editorial input from all authors. All authors read and approved the final manuscript.

AVAILABILITY OF DATA AND MATERIALS

The datasets used and analyzed during this study are available from the corresponding author on reasonable request.

REFERENCES

1. Bray, F. *et al.* Global cancer statistics 2018: GLOBOCAN estimates of incidence and mortality worldwide for 36 cancers in 185 countries. *CA. Cancer J. Clin.* **68**, 394–424 (2018).
2. Cancer of the Lung and Bronchus - Cancer Stat Facts. SEER.
3. Chargari, C. & Dhermain, F. Métastases cérébrales d'un cancer bronchique non à petites cellules : du traitement standardisé au traitement personnalisé. *Rev. Mal. Respir. Actual.* **5**, 547–556 (2013).
4. Tabouret, E. *et al.* Recent trends in epidemiology of brain metastases: an overview. *Anticancer Res.* **32**, 4655–4662 (2012).
5. Hall, W., Djalilian, H., Nussbaum, E. & Cho, K. Long-term survival with metastatic cancer to the brain. *Med. Oncol.* **17**, 279–286 (2000).
6. Gauger, J., Patz, E. F., Coleman, R. E. & Herndon, J. E. Clinical stage I non-small cell lung cancer including FDG-PET Imaging: sites and time to recurrence. *J. Thorac. Oncol. Off. Publ. Int. Assoc. Study Lung Cancer* **2**, 499–505 (2007).
7. Yano, T. *et al.* The first site of recurrence after complete resection in non-small-cell carcinoma of the lung. *J. Thorac. Cardiovasc. Surg.* **108**, 680–683 (1994).
8. Sadoyama, S. *et al.* Isolated Brain Metastases as the First Relapse After the Curative Surgical Resection in Non–Small-Cell Lung Cancer Patients With an EGFR Mutation. *Clin. Lung Cancer* **19**, e29–e36 (2018).
9. Figlin, R. A., Piantadosi, S., Feld, R., & The Lung Cancer Study Group*. Intracranial Recurrence of Carcinoma after Complete Surgical Resection of Stage I, II, and III Non-Small-Cell Lung Cancer. *N. Engl. J. Med.* **318**, 1300–1305 (1988).
10. ESMO. Metastatic Non-Small-Cell Lung Cancer: ESMO Clinical Practice Guidelines for diagnosis, treatment and follow-up. (2020).
11. Hellman, S. & Weichselbaum, R. R. Oligometastases. *J. Clin. Oncol. Off. J. Am. Soc. Clin. Oncol.* **13**, 8–10 (1995).
12. Laurie, S. A. *et al.* Canadian consensus: oligoprogressive, pseudoprogressive, and oligometastatic non-small-cell lung cancer. *Curr. Oncol. Tor. Ont* **26**, e81–e93 (2019).

13. Schoenmaekers, J. J. A. O., Paats, M. S., Dingemans, A.-M. C. & Hendriks, L. E. L. Central nervous system metastases and oligoprogression during treatment with tyrosine kinase inhibitors in oncogene-addicted non-small cell lung cancer: how to treat and when? *Transl. Lung Cancer Res.* **9**, 2599–2617 (2020).
14. Luca Ceresoli, G. *et al.* Brain metastases in locally advanced nonsmall cell lung carcinoma after multimodality treatment: Risk factors analysis. *Cancer* **95**, 605–612 (2002).
15. Zimm, S., Wampler, G. L., Stablein, D., Hazra, T. & Young, H. F. Intracerebral metastases in solid-tumor patients: natural history and results of treatment. *Cancer* **48**, 384–394 (1981).
16. Yamamoto, M. *et al.* Stereotactic radiosurgery for patients with multiple brain metastases (JLGK0901): a multi-institutional prospective observational study. *Lancet Oncol.* **15**, 387–395 (2014).
17. Zindler, J. D. *et al.* Whole brain radiotherapy versus stereotactic radiosurgery for 4-10 brain metastases: a phase III randomised multicentre trial. *BMC Cancer* **17**, 500 (2017).
18. Gerosa, M., Nicolato, A., Foroni, R., Tomazzoli, L. & Bricolo, A. Analysis of long-term outcomes and prognostic factors in patients with non-small cell lung cancer brain metastases treated by gamma knife radiosurgery. *J. Neurosurg.* **102 Suppl**, 75–80 (2005).
19. Motta, M. *et al.* Gamma knife radiosurgery for treatment of cerebral metastases from non-small-cell lung cancer. *Int. J. Radiat. Oncol. Biol. Phys.* **81**, e463-468 (2011).
20. Fuentes, R. *et al.* Surgery versus stereotactic radiotherapy for people with single or solitary brain metastasis. *Cochrane Database Syst. Rev.* **8**, CD012086 (2018).
21. Aupérin, A. *et al.* Prophylactic Cranial Irradiation for Patients with Small-Cell Lung Cancer in Complete Remission. *N. Engl. J. Med.* **341**, 476–484 (1999).
22. Liu, L. *et al.* The Role of Prophylactic Cranial Irradiation in Patients With Non-small Cell Lung Cancer: An Updated Systematic Review and Meta-Analysis. *Front. Oncol.* **10**, 11 (2020).
23. Chang, E. L. *et al.* Neurocognition in patients with brain metastases treated with radiosurgery or radiosurgery plus whole-brain irradiation: a randomised controlled trial. *Lancet Oncol.* **10**, 1037–1044 (2009).
24. Soffietti, R. *et al.* A European Organisation for Research and Treatment of Cancer phase III trial of adjuvant whole-brain radiotherapy versus observation in patients with one to three brain metastases from solid tumors after surgical resection or radiosurgery: quality-of-life results. *J. Clin. Oncol. Off. J. Am. Soc. Clin. Oncol.* **31**, 65–72 (2013).

25. Besse, B. *et al.* Bevacizumab in Patients with Nonsquamous Non-Small Cell Lung Cancer and Asymptomatic, Untreated Brain Metastases (BRAIN): A Nonrandomized, Phase II Study. *Clin. Cancer Res. Off. J. Am. Assoc. Cancer Res.* **21**, 1896–1903 (2015).
26. Socinski, M. A. *et al.* Atezolizumab for First-Line Treatment of Metastatic Nonsquamous NSCLC. *N. Engl. J. Med.* **378**, 2288–2301 (2018).
27. Reck, M. *et al.* Pembrolizumab versus Chemotherapy for PD-L1–Positive Non–Small-Cell Lung Cancer. *N. Engl. J. Med.* **375**, 1823–1833 (2016).
28. Gandhi, L. *et al.* Pembrolizumab plus Chemotherapy in Metastatic Non–Small-Cell Lung Cancer. *N. Engl. J. Med.* **378**, 2078–2092 (2018).
29. Sweeney, M. D., Zhao, Z., Montagne, A., Nelson, A. R. & Zlokovic, B. V. Blood-Brain Barrier: From Physiology to Disease and Back. *Physiol. Rev.* **99**, 21–78 (2019).
30. Cortinovis, D. *et al.* Italian Cohort of the Nivolumab EAP in Squamous NSCLC: Efficacy and Safety in Patients With CNS Metastases. *Anticancer Res.* **39**, 4265–4271 (2019).
31. Dudnik, E. *et al.* Intracranial response to nivolumab in NSCLC patients with untreated or progressing CNS metastases. *Lung Cancer Amst. Neth.* **98**, 114–117 (2016).
32. Goldberg, S. B. *et al.* Pembrolizumab for patients with melanoma or non-small-cell lung cancer and untreated brain metastases: early analysis of a non-randomised, open-label, phase 2 trial. *Lancet Oncol.* **17**, 976–983 (2016).
33. Gauvain, C. *et al.* Intracerebral efficacy and tolerance of nivolumab in non–small-cell lung cancer patients with brain metastases. *Lung Cancer* **116**, 62–66 (2018).
34. Leighl, N. B. *et al.* CCTG BR.34: A randomized trial of durvalumab and tremelimumab +/- platinum-based chemotherapy in patients with metastatic (Stage IV) squamous or nonsquamous non-small cell lung cancer (NSCLC). *J. Clin. Oncol.* **38**, 9502–9502 (2020).
35. Powell, S. F. *et al.* Pembrolizumab (pembro) plus platinum-based chemotherapy (chemo) in NSCLC with brain metastases: Pooled analysis of KEYNOTE-021, 189, and 407. *Ann. Oncol.* **30**, v606–v607 (2019).
36. Wang, X., Xu, Y., Tang, W. & Liu, L. Efficacy and Safety of Radiotherapy Plus EGFR-TKIs in NSCLC Patients with Brain Metastases: A Meta-Analysis of Published Data. *Transl. Oncol.* **11**, 1119–1127 (2018).

37. Levy, A. *et al.* Diversity of brain metastases screening and management in non-small cell lung cancer in Europe: Results of the European Organisation for Research and Treatment of Cancer Lung Cancer Group survey. *Eur. J. Cancer* **93**, 37–46 (2018).
38. Gaspar, L. *et al.* Recursive partitioning analysis (RPA) of prognostic factors in three radiation therapy oncology group (RTOG) brain metastases trials. *Int. J. Radiat. Oncol.* **37**, 745–751 (1997).
39. Sperduto, P. W. *et al.* Secondary analysis of RTOG 9508, a phase 3 randomized trial of whole-brain radiation therapy versus WBRT plus stereotactic radiosurgery in patients with 1-3 brain metastases; poststratified by the graded prognostic assessment (GPA). *Int. J. Radiat. Oncol. Biol. Phys.* **90**, 526–531 (2014).
40. Sperduto, P. W. *et al.* Estimating Survival in Patients With Lung Cancer and Brain Metastases: An Update of the Graded Prognostic Assessment for Lung Cancer Using Molecular Markers (Lung-molGPA). *JAMA Oncol.* **3**, 827–831 (2017).
41. Bajard, A. *et al.* Multivariate analysis of factors predictive of brain metastases in localised non-small cell lung carcinoma. *Lung Cancer* **45**, 317–323 (2004).
42. Hayashi, N. *et al.* Negative impact of leukoaraiosis on the incidence of brain metastases in patients with lung cancer. *J. Neurooncol.* **135**, 299–306 (2017).
43. Liotta, L. A., Saidel, G. M. & Kleinerman, J. Stochastic model of metastases formation. *Biometrics* **32**, 535–550 (1976).
44. Hartung, N. *et al.* Mathematical Modeling of Tumor Growth and Metastatic Spreading: Validation in Tumor-Bearing Mice. *Cancer Res.* **74**, 6397–6407 (2014).
45. Baratchart, E. *et al.* Computational Modelling of Metastasis Development in Renal Cell Carcinoma. *PLoS Comput. Biol.* **11**, e1004626 (2015).
46. Benzekry, S. *et al.* Modeling Spontaneous Metastasis following Surgery: An In Vivo-In Silico Approach. *Cancer Res.* **76**, 535–547 (2016).
47. Laird, A. K. DYNAMICS OF TUMOUR GROWTH: COMPARISON OF GROWTH RATES AND EXTRAPOLATION OF GROWTH CURVE TO ONE CELL. *Br. J. Cancer* **19**, 278–291 (1965).
48. Norton, L. A Gompertzian model of human breast cancer growth. *Cancer Res.* **48**, 7067–7071 (1988).
49. Benzekry, S. *et al.* Classical Mathematical Models for Description and Prediction of Experimental Tumor Growth. *PLoS Comput. Biol.* **10**, e1003800 (2014).

50. Iwata, K., Kawasaki, K. & Shigesada, N. A dynamical model for the growth and size distribution of multiple metastatic tumors. *J. Theor. Biol.* **203**, 177–186 (2000).

51. Schlicke, P., Kuttler, C. & Schumann, C. How mathematical modeling could contribute to the quantification of metastatic tumor burden under therapy: insights in immunotherapeutic treatment of non-small cell lung cancer. *Theor. Biol. Med. Model.* **18**, 11 (2021).

52. Nicolò, C. *et al.* Machine Learning and Mechanistic Modeling for Prediction of Metastatic Relapse in Early-Stage Breast Cancer. *JCO Clin. Cancer Inform.* 259–274 (2020) doi:10.1200/CCI.19.00133.

53. Cooley, L. S. *et al.* Experimental and computational modeling for signature and biomarker discovery of renal cell carcinoma progression. *Mol. Cancer* **20**, 136 (2021).

54. Bilous, M. *et al.* Quantitative mathematical modeling of clinical brain metastasis dynamics in non-small cell lung cancer. *Sci. Rep.* **9**, 13018 (2019).

55. Spratt, J. S., Meyer, J. S. & Spratt, J. A. Rates of growth of human solid neoplasms: Part I. *J. Surg. Oncol.* **60**, 137–146 (1995).

56. On the nature of the function expressive of the law of human mortality, and on a new mode of determining the value of life contingencies. In a letter to Francis Baily, Esq. F. R. S. &c. By Benjamin Gompertz, Esq. F. R. S. *Abstr. Pap. Print. Philos. Trans. R. Soc. Lond.* **2**, 252–253 (1833).

57. Casey, A. E. The Experimental Alteration of Malignancy with an Homologous Mammalian Tumor Material: I. Results with Intratesticular Inoculation. *Am. J. Cancer* **21**, 760 (1934).

58. Benzekry, S. *et al.* Classical Mathematical Models for Description and Prediction of Experimental Tumor Growth. *PLoS Comput. Biol.* **10**, e1003800 (2014).

59. Vaghi, C. *et al.* Population modeling of tumor growth curves and the reduced Gompertz model improve prediction of the age of experimental tumors. *PLOS Comput. Biol.* **16**, e1007178 (2020).

60. Bilous, M. *et al.* Quantitative mathematical modeling of clinical brain metastasis dynamics in non-small cell lung cancer. *Sci. Rep.* **9**, 13018 (2019).

61. Bethge, A., Schumacher, U., Wree, A. & Wedemann, G. Are Metastases from Metastases Clinical Relevant? Computer Modelling of Cancer Spread in a Case of Hepatocellular Carcinoma. *PLoS ONE* **7**, e35689 (2012).

62. Klein, C. A. Parallel progression of primary tumours and metastases. *Nat. Rev. Cancer* **9**, 302–312 (2009).

63. MathWorks: MATLAB Documentary GlobalSearch.

64. Ugray, Z. *et al.* Scatter Search and Local NLP Solvers: A Multistart Framework for Global Optimization. *Inf. J. Comput.* **19**, 328–340 (2007).

65. Benzekry, S., Sentis, C., Coze, C., Tessonnier, L. & André, N. Development and Validation of a Prediction Model of Overall Survival in High-Risk Neuroblastoma Using Mechanistic Modeling of Metastasis. *JCO Clin. Cancer Inform.* 81–90 (2021) doi:10.1200/CCI.20.00092.

66. Bland, J. M. & Altman, D. G. The logrank test. *BMJ* **328**, 1073 (2004).

67. Davidson-Pilon, C. lifelines: survival analysis in Python. *J. Open Source Softw.* **4**, 1317 (2019).

68. Harrell, F. E., Lee, K. L. & Mark, D. B. Multivariable prognostic models: issues in developing models, evaluating assumptions and adequacy, and measuring and reducing errors. *Stat. Med.* **15**, 361–387 (1996).

69. Pope, W. B. Brain metastases: neuroimaging. in *Handbook of Clinical Neurology* vol. 149 89–112 (Elsevier, 2018).

70. Brindle, K. M., Izquierdo-García, J. L., Lewis, D. Y., Mair, R. J. & Wright, A. J. Brain Tumor Imaging. *J. Clin. Oncol.* **35**, 2432–2438 (2017).

71. Azin, M. & Demehri, S. STK11 Loss: A Novel Mechanism for Melanoma Metastasis with Therapeutic Implications. *J. Invest. Dermatol.* **142**, 1007–1009 (2022).

72. Huang, D. *et al.* Mutations of key driver genes in colorectal cancer progression and metastasis. *Cancer Metastasis Rev.* **37**, 173–187 (2018).

73. Wikman, H. *et al.* Relevance of PTEN loss in brain metastasis formation in breast cancer patients. *Breast Cancer Res.* **14**, R49 (2012).

74. Lohmann, P. *et al.* PET/MRI Radiomics in Patients With Brain Metastases. *Front. Neurol.* **11**, 1 (2020).

75. Zhao, S. *et al.* MRI radiomic signature predicts intracranial progression-free survival in patients with brain metastases of ALK-positive non-small cell lung cancer. *Transl. Lung Cancer Res.* **10**, 368–380 (2021).

76. Huang, C.-Y. *et al.* Radiomics as prognostic factor in brain metastases treated with Gamma Knife radiosurgery. *J. Neurooncol.* **146**, 439–449 (2020).

77. Zhang, J. *et al.* Computer Tomography Radiomics-Based Nomogram in the Survival Prediction for Brain Metastases From Non-Small Cell Lung Cancer Underwent Whole Brain Radiotherapy. *Front. Oncol.* **10**, 610691 (2021).

78. Perlikos, F., Harrington, K. J. & Syrigos, K. N. Key molecular mechanisms in lung cancer invasion and metastasis: A comprehensive review. *Crit. Rev. Oncol. Hematol.* **87**, 1–11 (2013).

79. Nakamura, R. *et al.* Epidermal Growth Factor Receptor Mutations: Effect on Volume Doubling Time of Non–Small-Cell Lung Cancer Patients. *J. Thorac. Oncol.* **9**, 1340–1344 (2014).

80. Zhang, R. *et al.* Volume doubling time of lung adenocarcinomas considering epidermal growth factor receptor mutation status of exon 19 and 21: three-dimensional volumetric evaluation. *J. Thorac. Dis.* **9**, 4387–4397 (2017).

81. Robin, T. P. *et al.* Excellent Outcomes with Radiosurgery for Multiple Brain Metastases in ALK and EGFR Driven Non–Small Cell Lung Cancer. *J. Thorac. Oncol.* **13**, 715–720 (2018).

82. Wu, Y.-L. *et al.* Osimertinib in Resected *EGFR* -Mutated Non–Small-Cell Lung Cancer. *N. Engl. J. Med.* **383**, 1711–1723 (2020).

83. Forde, P. M. *et al.* Neoadjuvant Nivolumab plus Chemotherapy in Resectable Lung Cancer. *N. Engl. J. Med.* NEJMoa2202170 (2022) doi:10.1056/NEJMoa2202170.

84. Felip, E. *et al.* Adjuvant atezolizumab after adjuvant chemotherapy in resected stage IB–IIIA non-small-cell lung cancer (IMpower010): a randomised, multicentre, open-label, phase 3 trial. *The Lancet* **398**, 1344–1357 (2021).

85. Endo, H. & Inoue, M. Dormancy in cancer. *Cancer Sci.* **110**, 474–480 (2019).

86. Bethge, A., Schumacher, U., Wree, A. & Wedemann, G. Are Metastases from Metastases Clinical Relevant? Computer Modelling of Cancer Spread in a Case of Hepatocellular Carcinoma. *PLoS ONE* **7**, e35689 (2012).

87. Quail, D. F. & Joyce, J. A. The Microenvironmental Landscape of Brain Tumors. *Cancer Cell* **31**, 326–341 (2017).

SUPPLEMENTARY MATERIAL

S1: Analytical solution of the primary tumor and metastases' growth dynamics

A primary tumor (PT) with size $S_P(t)$ at time $t \geq 0$ was assumed to follow Gompertzian growth[56,57]. Since patients underwent surgery, we adjusted the growth equation to account for full tumor removal at day of surgery $T_s > 0$ such that

$$\frac{dS_P(t)}{dt} = g_P\big(S_P(t)\big) = \big(\alpha_P - \beta_P \ln(S_P)\big)S_P, \text{ if } 0 < t \leq T_S$$

but $S_P(t) = 0$ if $t > T_S$.

Variables and parameters are explained in the text. The analytical solution to the primary tumor dynamics can be determined to be

$$S_P(t) = \begin{cases} exp\left(\frac{\alpha_P}{\beta_P}\big(1 - exp(-\beta_P t)\big)\right), \text{ if } 0 \leq t \leq T_S \\ 0 \qquad\qquad\qquad\qquad\quad , \text{ if } t > T_S. \end{cases}$$

and the metastases' Gompertz growth function is given analogously, without the possible surgery modelled, as

$$g_m(s) = (\alpha - \beta \ln(s))s.$$

Therefore, α and β correspond to the BM growth parameters. The BM Gompertzian formula is the analytical solution of the equation

$$\frac{ds(t)}{dt} = g_m(s).$$

with initial condition $s(0) = 1$ that describes the metastatic size s at time $t \geq 0$, i.e.:

$$s(t) = exp\left(\frac{\alpha}{\beta}(1 - \exp(-\beta t))\right).$$

S2: Model equation for the metastatic density $\rho(s,t)$ of size s and time t

The full equation corresponding to the approach of [60] modelling the metastatic density $\rho(s,t)$ as function of size s and time t with boundary and initial conditions neglecting secondary metastasis – not considering the integral in the boundary condition – reads

$$\frac{\partial\rho(s,t)}{\partial t}+\frac{\partial(g_m(s)\rho(s,t))}{\partial s}=0$$
$$g(1)\rho(1,t)=\mu S_P(t)^\gamma$$
$$\rho(x,0)=0$$

The two parameters governing BM dissemination are therefore γ and μ. The first – γ – controls the repartition of PT cells with metastatic potential (e.g., $\gamma=1$ means all cells within the tumor have equal probability of leading to a BM, $\gamma=2/3$ means only the cells at the surface have metastatic propensity). The second – μ – represents the per time unit probability of each PT cells with BM potential to actually lead to a BM.

S3: Numerical implementation: calculate metastases

Since we assumed that the primary tumor was the only source for metastases, we applied a previously detailed procedure to calculate the absolute number of metastases $N(t)$ at time t, given individual parameters $(\alpha_P,\beta_P,\alpha,\beta,\mu,\gamma)$ [60]:

$$N(t)=\int_0^t \mu\, S_P(\tau)^\gamma d\tau.$$

We then introduce the cumulative size distribution $f(t,s)$ as the number of metastases larger than a fixed size s at t (cumulative size distribution):

$$f(t,s)=\int_s^{\exp\left(\frac{\alpha}{\beta}\right)}\rho\,(t,\sigma)d\sigma.$$

Denoting $t(s)$ the time for a tumor to reach size s under Gompertz growth we have[60]

$$f(t,s)=N\big(t-t(s)\big),$$

with

$$t(s)=-\frac{1}{\beta}\ln\left(1-\frac{\beta}{\alpha}\ln(s)\right).$$

The cumulative distribution $f(t,s)$ can be compared to the clinical data by assuming that the visible BMs correspond to the BMs larger than the volume corresponding to a diameter measurement of three mm, that we denote s_v. Thus, the model-derived number of visible metastases is defined by $f(t,s_v)$.

S4: Parameter estimation: primary tumor growth parameters

The doubling time $\tau_P(s)$ of a primary tumor of size $S_P(T_d)$ at time of diagnosis $0\le T_d\le T_S$, i.e. the time a tumor of size s needs to grow to a size of $2s$, is implicitly given by[51]

$$\tau_P(s)=-\frac{1}{\beta_P}\ln\left(\frac{\beta_P\ln(2S_P)-\alpha_P}{\beta_P\ln(S_P)-\alpha_P}\right)$$

and from $exp(\alpha_P/\beta_P) = 10^{12}$ we determined the parameters α_P and β_P from the primary tumor histology and the primary tumor size at diagnosis. Since on the other hand $exp(\alpha/\beta) = 10^{12}$ for the metastases' dynamics, the parameter β was determined from the value of parameter α, which in turn was a fitted parameter (cf. below).

S5: Parameter identification from the data

Following the previous considerations, three parameters remained to be specified: (α, μ, γ). Preliminary exploration of the parameter space suggested that a value of $\gamma = 0.1$ was able to describe the data. Therefore, in order to ensure parametric identifiability, we fixed this parameter value to 0.1 for all patients.

To determine the size and number of BMs from the model equations and values, we only used data up to the time of first metastatic relapse – denoted T_{BM} – and consequently identified the parameters using only one time point with BMs measurements.

In this context, parameter identification was highly unstable.

Two scenarios were therefore considered. In the first, all BMs above the visible threshold s_v were assumed to have been detected. In the second, we accounted for the possibility that some were not. Our final method is a compromise between the two scenarios. We assumed an artificial "half" BM with size s_v, that is, it accounts for a half BM, corresponding to a 0.5 probability to be in either the first or second scenario. Using this method allowed us to control the important variance of the metastatic density below s_v.

A least squares calculation comparing model evaluations of $f(T_{BM}, s)$ (cumulative BM size distribution) against the empirical data using the GlobalSearch environment[63,64], fitting for the two parameters α and μ on biologically reasonable intervals (i.e. positive values).

S6: Model simulations for every individual patient of the data set

The explanation of every subpanel is given in the description of figure 3 of the main text.

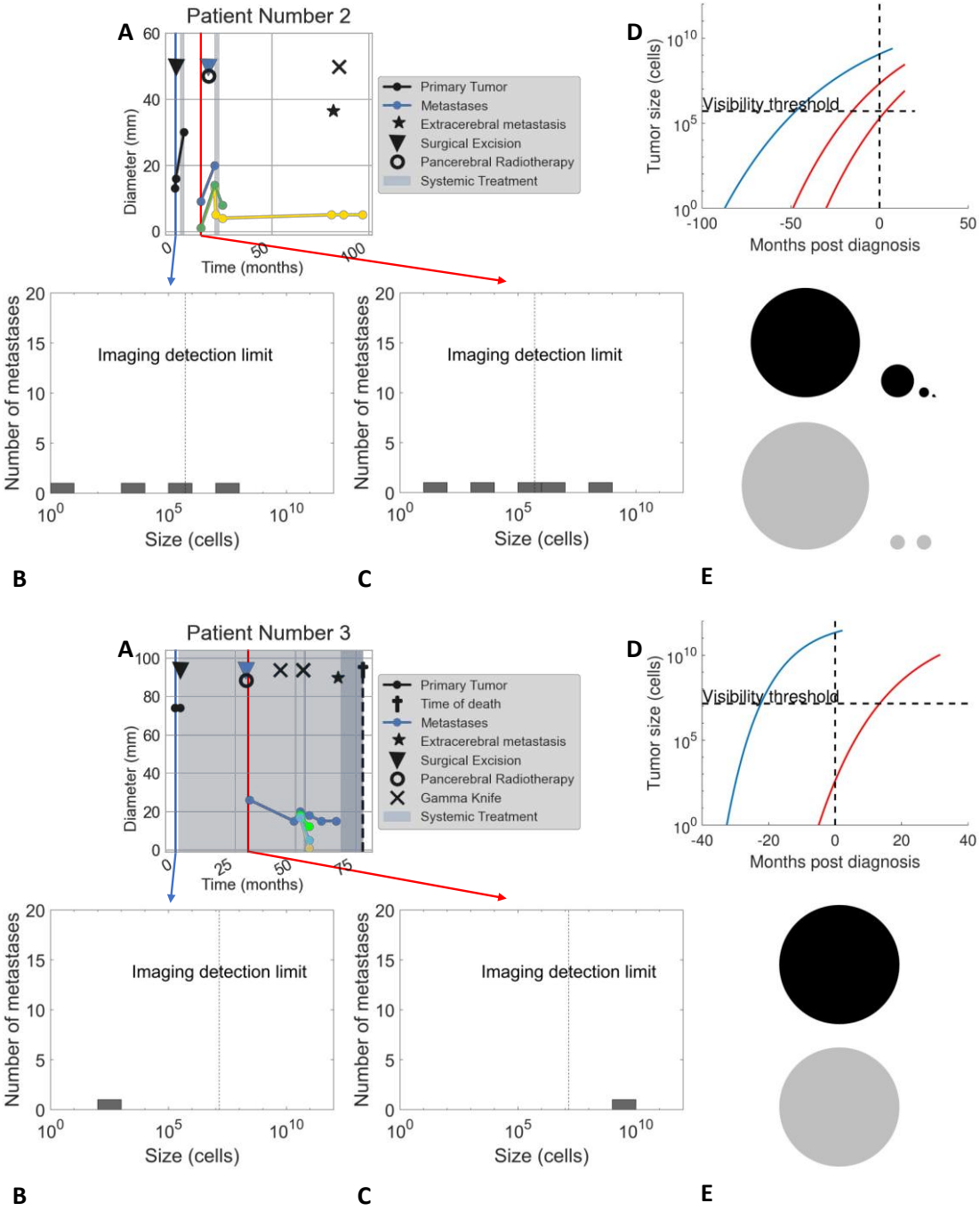

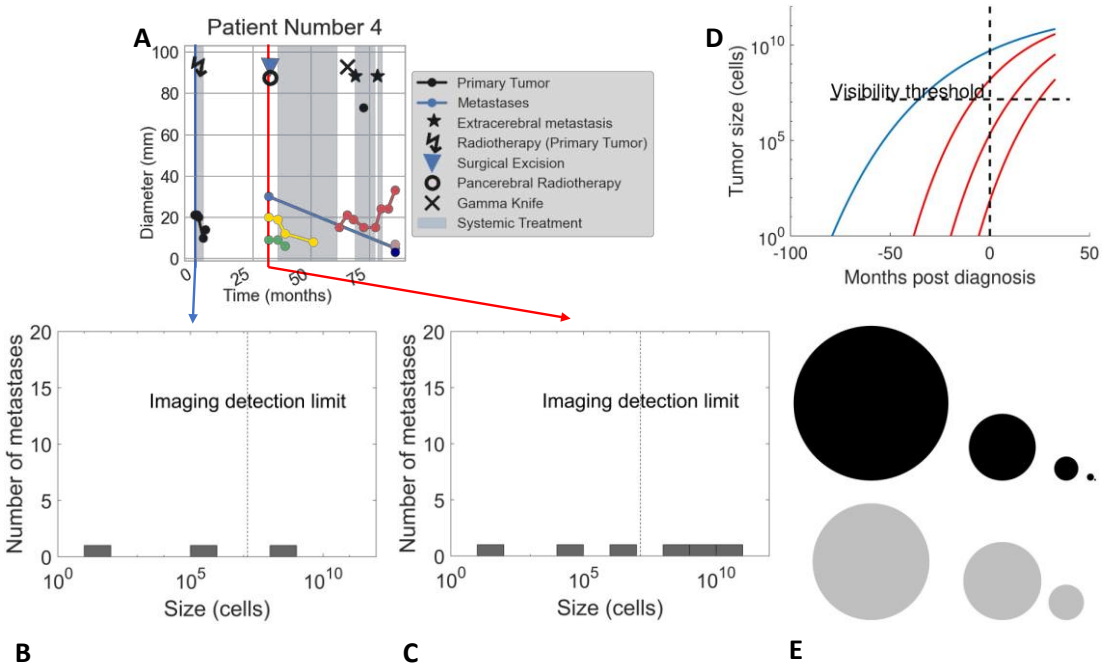
A
Patient Number 4
Diameter (mm)
Time (months)
Primary Tumor
Metastases
Extracerebral metastasis
Radiotherapy (Primary Tumor)
Surgical Excision
Pancerebral Radiotherapy
Gamma Knife
Systemic Treatment
D
Tumor size (cells)
Visibility threshold
Months post diagnosis
B
Number of metastases
Imaging detection limit
Size (cells)
C
Number of metastases
Imaging detection limit
Size (cells)
E

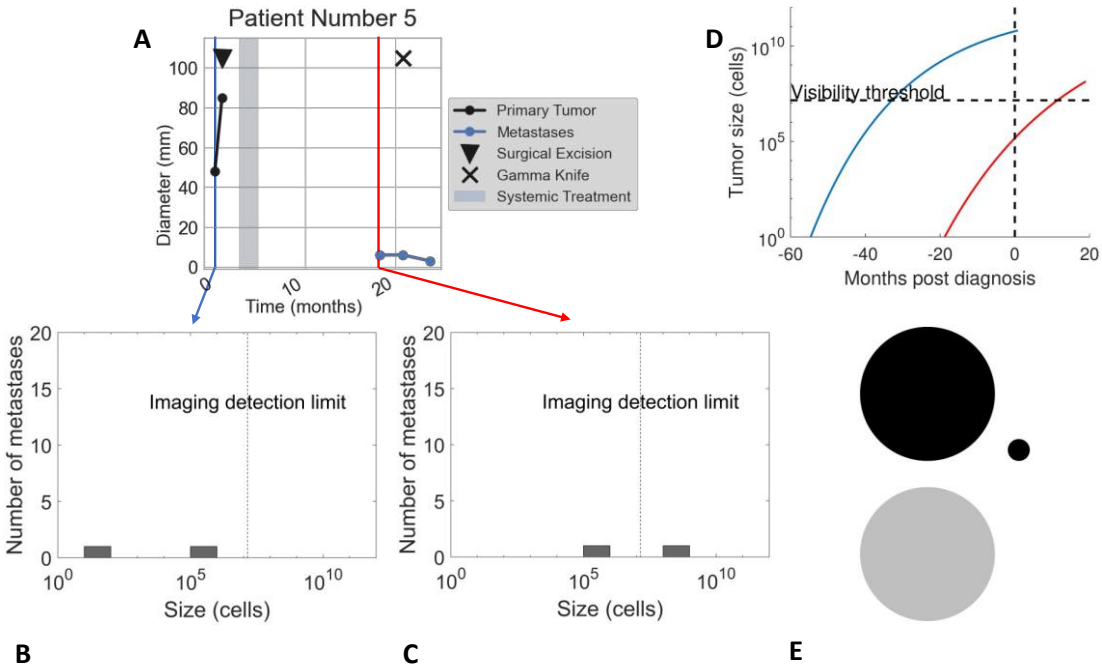
A
Patient Number 5
Diameter (mm)
Time (months)
Primary Tumor
Metastases
Surgical Excision
Gamma Knife
Systemic Treatment
D
Tumor size (cells)
Visibility threshold
Months post diagnosis
B
Number of metastases
Imaging detection limit
Size (cells)
C
Number of metastases
Imaging detection limit
Size (cells)
E

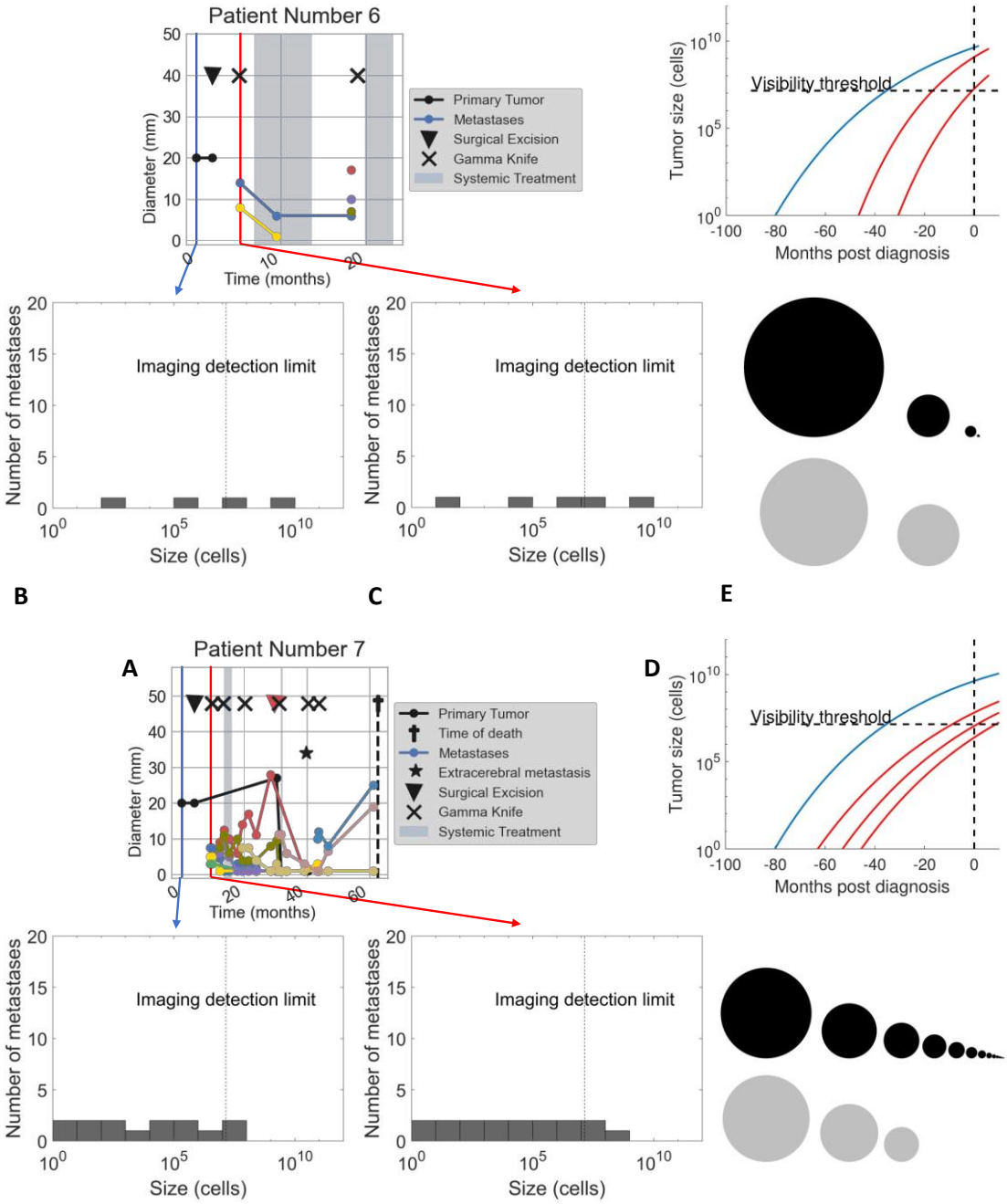
Patient Number 6
Diameter (mm)
Time (months)
Primary Tumor
Metastases
Surgical Excision
Gamma Knife
Systemic Treatment
Tumor size (cells)
Visibility threshold
Months post diagnosis
Number of metastases
Imaging detection limit
Size (cells)
B
C
E
A
Patient Number 7
Time of death
Extracerebral metastasis
D

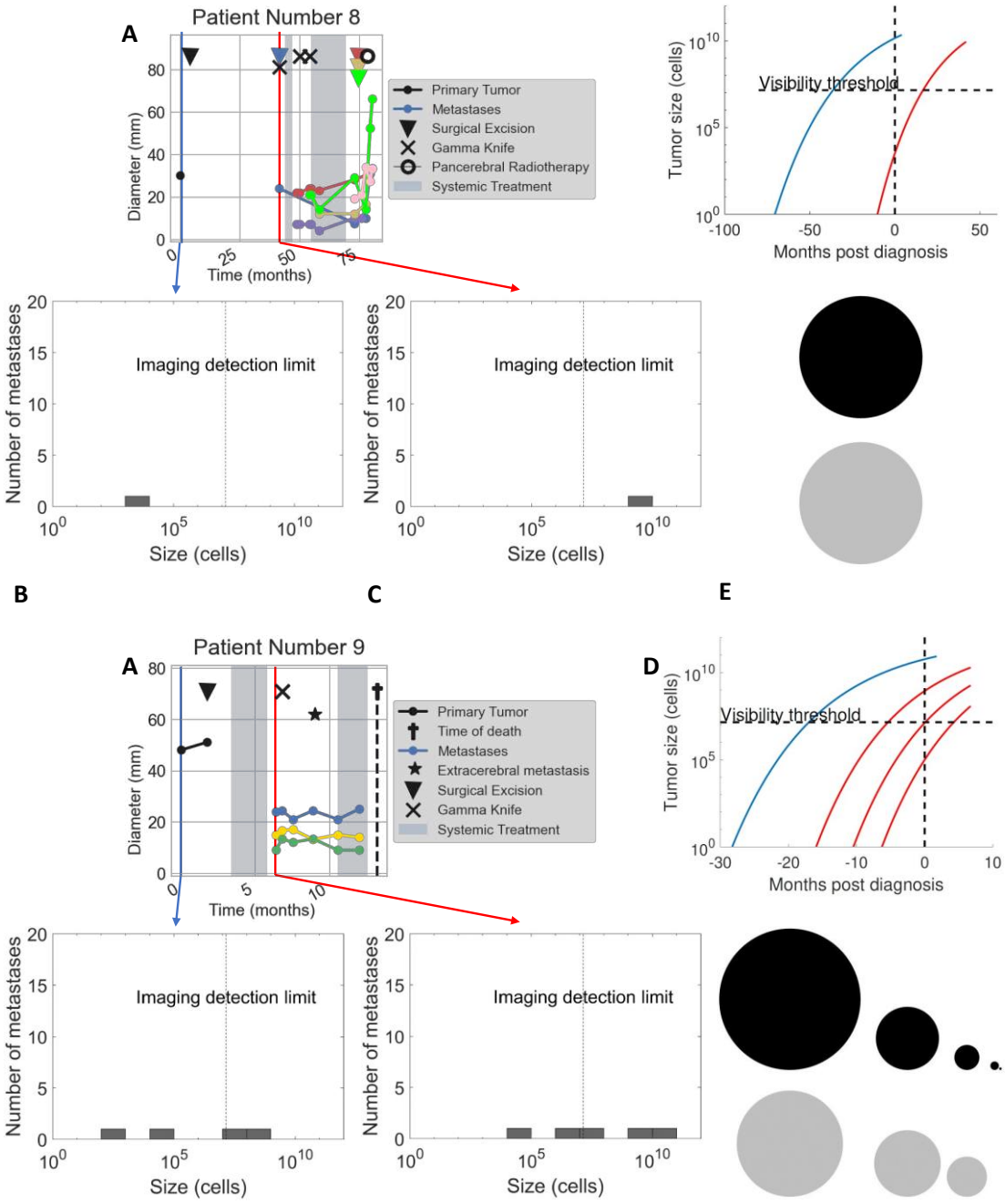
A
Patient Number 8
Diameter (mm)
Time (months)
Primary Tumor
Metastases
Surgical Excision
Gamma Knife
Pancerebral Radiotherapy
Systemic Treatment
Tumor size (cells)
Visibility threshold
Months post diagnosis
Number of metastases
Imaging detection limit
Size (cells)
B
C
E
A
Patient Number 9
Diameter (mm)
Time (months)
Primary Tumor
Time of death
Metastases
Extracerebral metastasis
Surgical Excision
Gamma Knife
Systemic Treatment
D
Tumor size (cells)
Visibility threshold
Months post diagnosis
Number of metastases
Imaging detection limit
Size (cells)

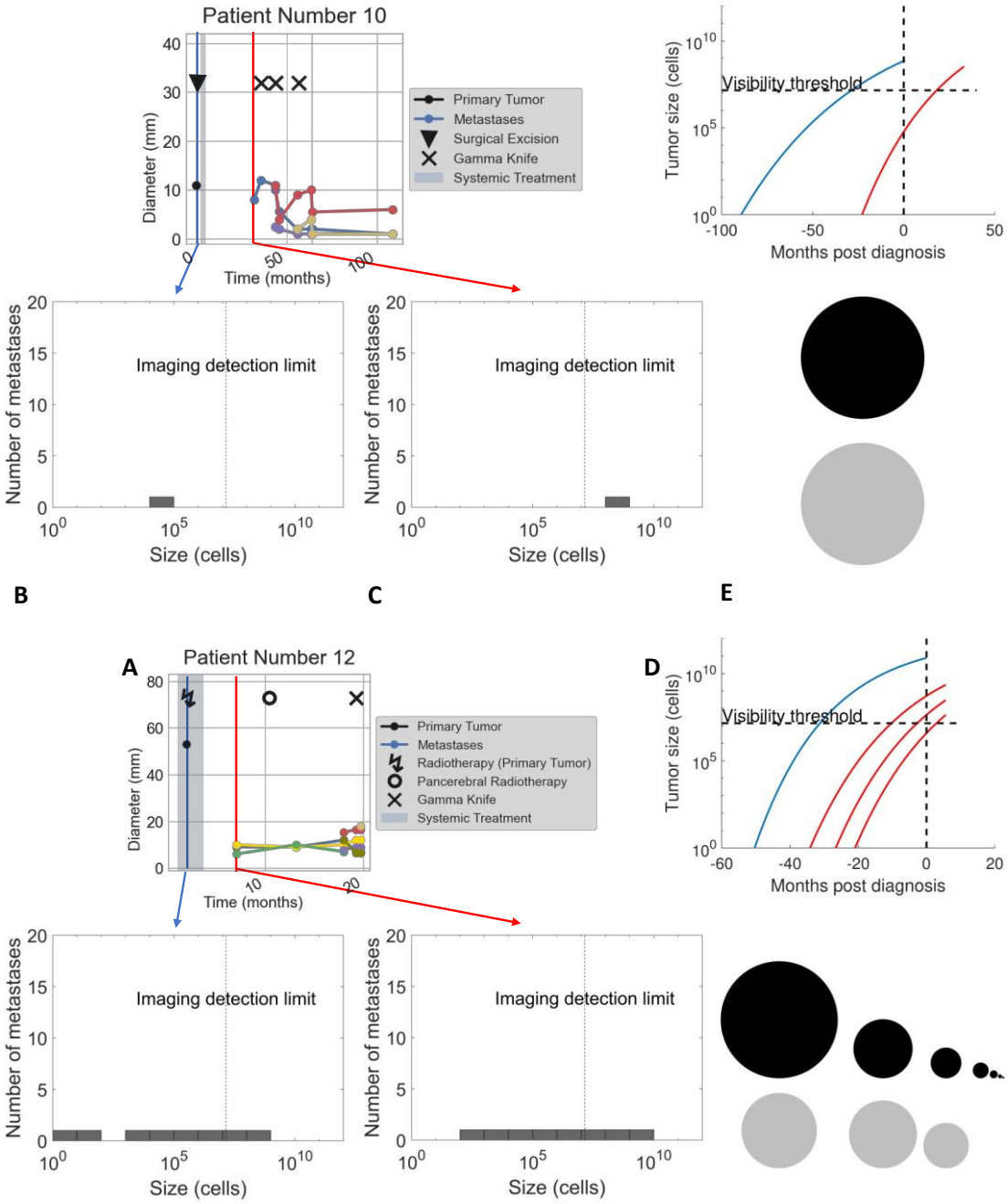
Patient Number 10
Diameter (mm)
Time (months)
Primary Tumor
Metastases
Surgical Excision
Gamma Knife
Systemic Treatment
Tumor size (cells)
Visibility threshold
Months post diagnosis
Number of metastases
Imaging detection limit
Size (cells)
B
C
E
A
Patient Number 12
Radiotherapy (Primary Tumor)
Pancerebral Radiotherapy
D

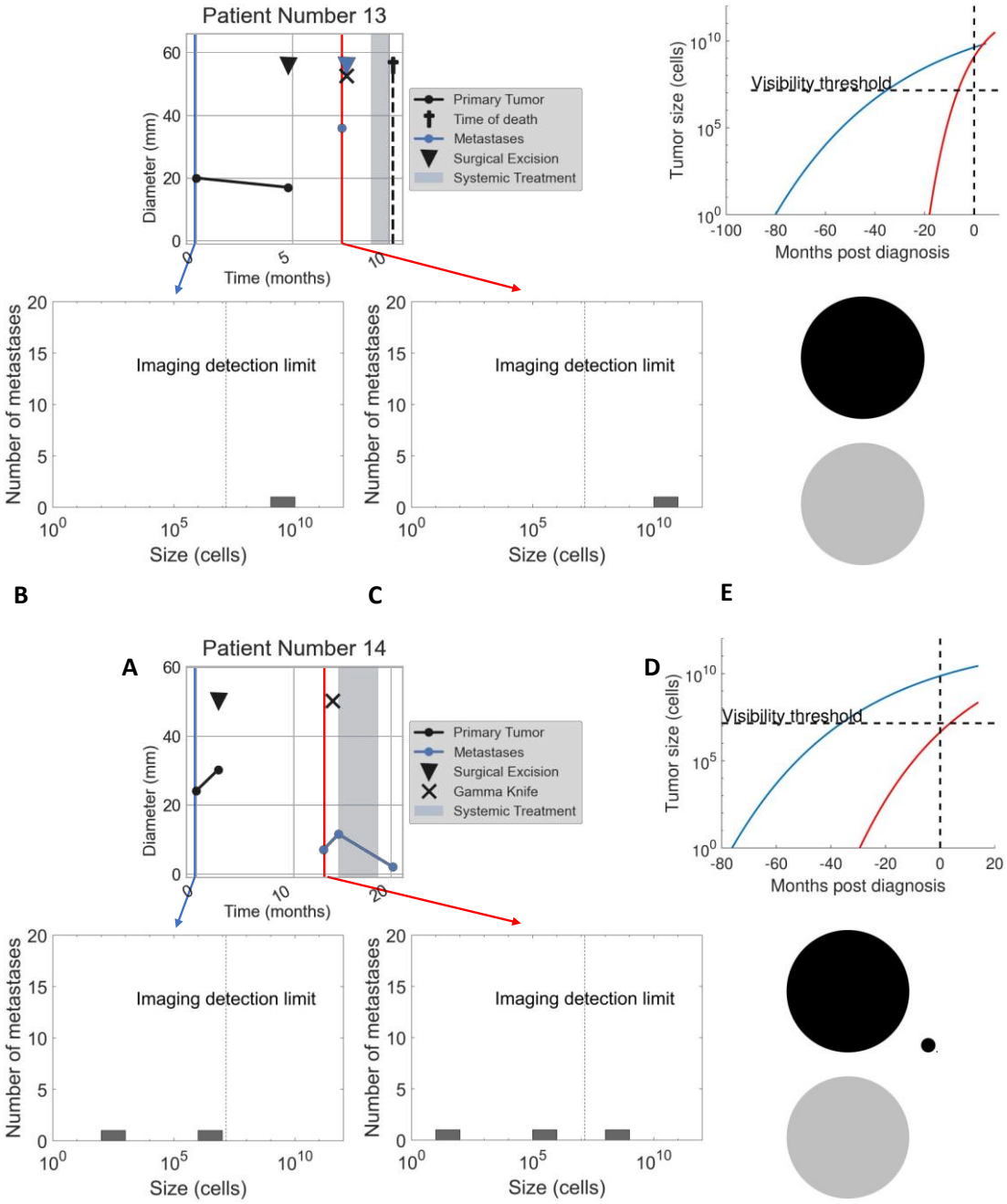
Patient Number 13
Diameter (mm)
Time (months)
Primary Tumor
Time of death
Metastases
Surgical Excision
Systemic Treatment
Tumor size (cells)
Visibility threshold
Months post diagnosis
Number of metastases
Imaging detection limit
Size (cells)
B
C
E
A
Patient Number 14
Gamma Knife
D

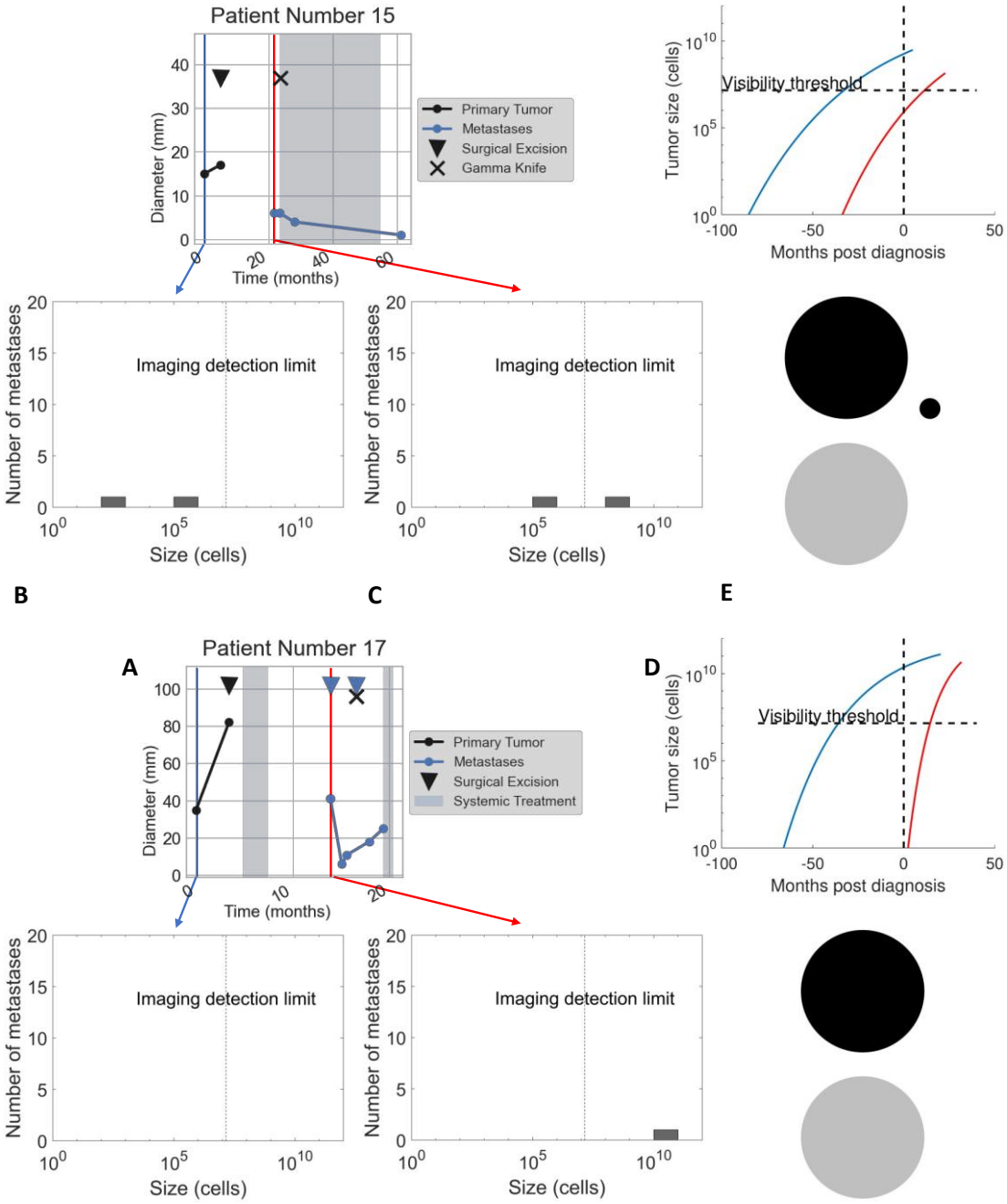
Patient Number 15
Diameter (mm)
Time (months)
Primary Tumor
Metastases
Surgical Excision
Gamma Knife
Tumor size (cells)
Visibility threshold
Months post diagnosis
Number of metastases
Imaging detection limit
Size (cells)
B
C
E
A
Patient Number 17
Systemic Treatment
D

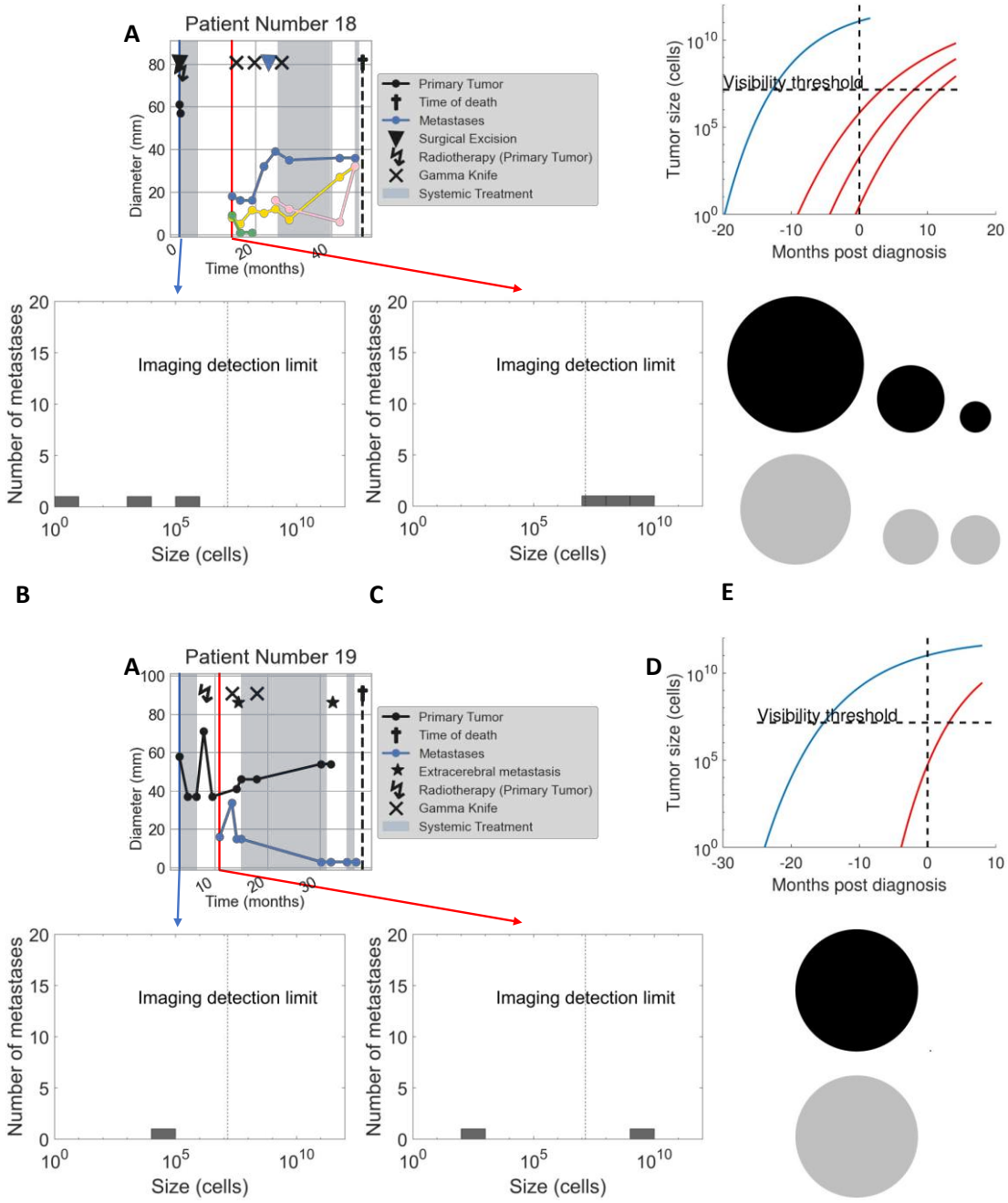
A
Patient Number 18
Diameter (mm)
Time (months)
Primary Tumor
Time of death
Metastases
Surgical Excision
Radiotherapy (Primary Tumor)
Gamma Knife
Systemic Treatment
Tumor size (cells)
Visibility threshold
Months post diagnosis
Number of metastases
Imaging detection limit
Size (cells)
B
C
E
A
Patient Number 19
Diameter (mm)
Time (months)
Primary Tumor
Time of death
Metastases
Extracerebral metastasis
Radiotherapy (Primary Tumor)
Gamma Knife
Systemic Treatment
D
Tumor size (cells)
Visibility threshold
Months post diagnosis
Number of metastases
Imaging detection limit
Size (cells)

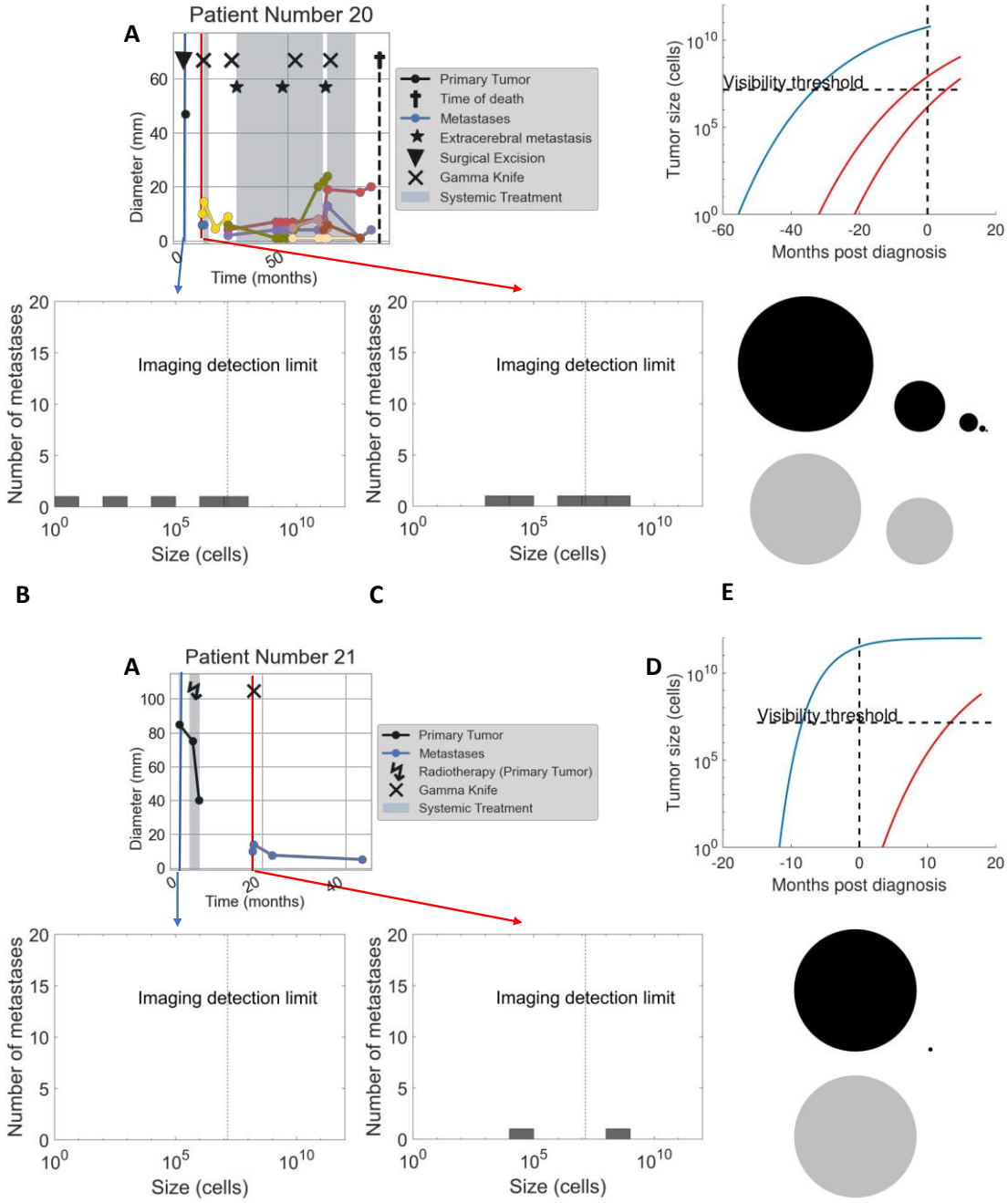
A
Patient Number 20
Diameter (mm)
Time (months)
Primary Tumor
Time of death
Metastases
Extracerebral metastasis
Surgical Excision
Gamma Knife
Systemic Treatment
Tumor size (cells)
Visibility threshold
Months post diagnosis
Number of metastases
Imaging detection limit
Size (cells)
B
C
E
A
Patient Number 21
Diameter (mm)
Time (months)
Primary Tumor
Metastases
Radiotherapy (Primary Tumor)
Gamma Knife
Systemic Treatment
D
Tumor size (cells)
Visibility threshold
Months post diagnosis
Number of metastases
Imaging detection limit
Size (cells)

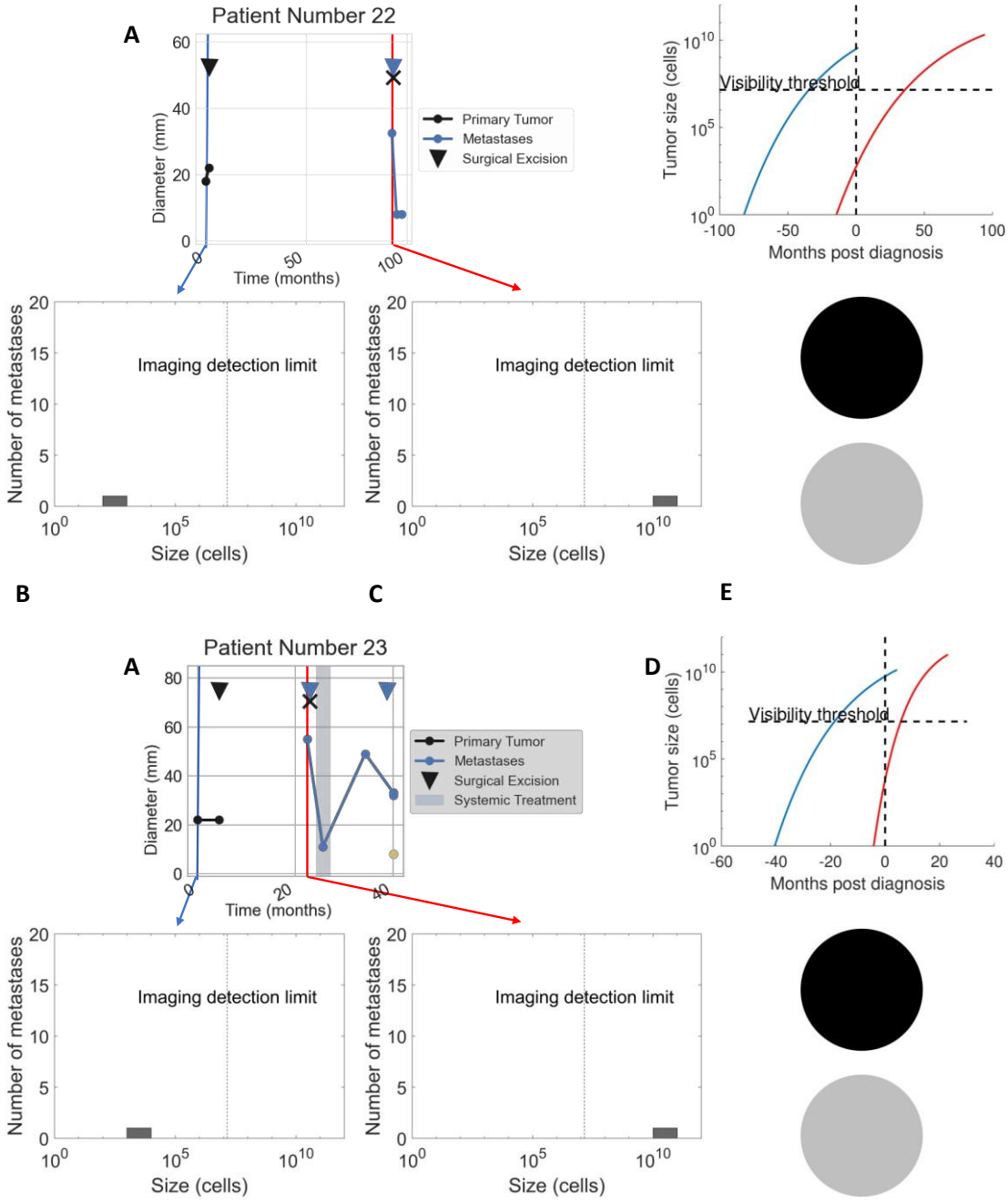
A
Patient Number 22
Diameter (mm)
Time (months)
Primary Tumor
Metastases
Surgical Excision
Tumor size (cells)
Visibility threshold
Months post diagnosis
Number of metastases
Imaging detection limit
Size (cells)
B
C
E
A
Patient Number 23
Diameter (mm)
Time (months)
Primary Tumor
Metastases
Surgical Excision
Systemic Treatment
D
Tumor size (cells)
Visibility threshold
Months post diagnosis
Number of metastases
Imaging detection limit
Size (cells)

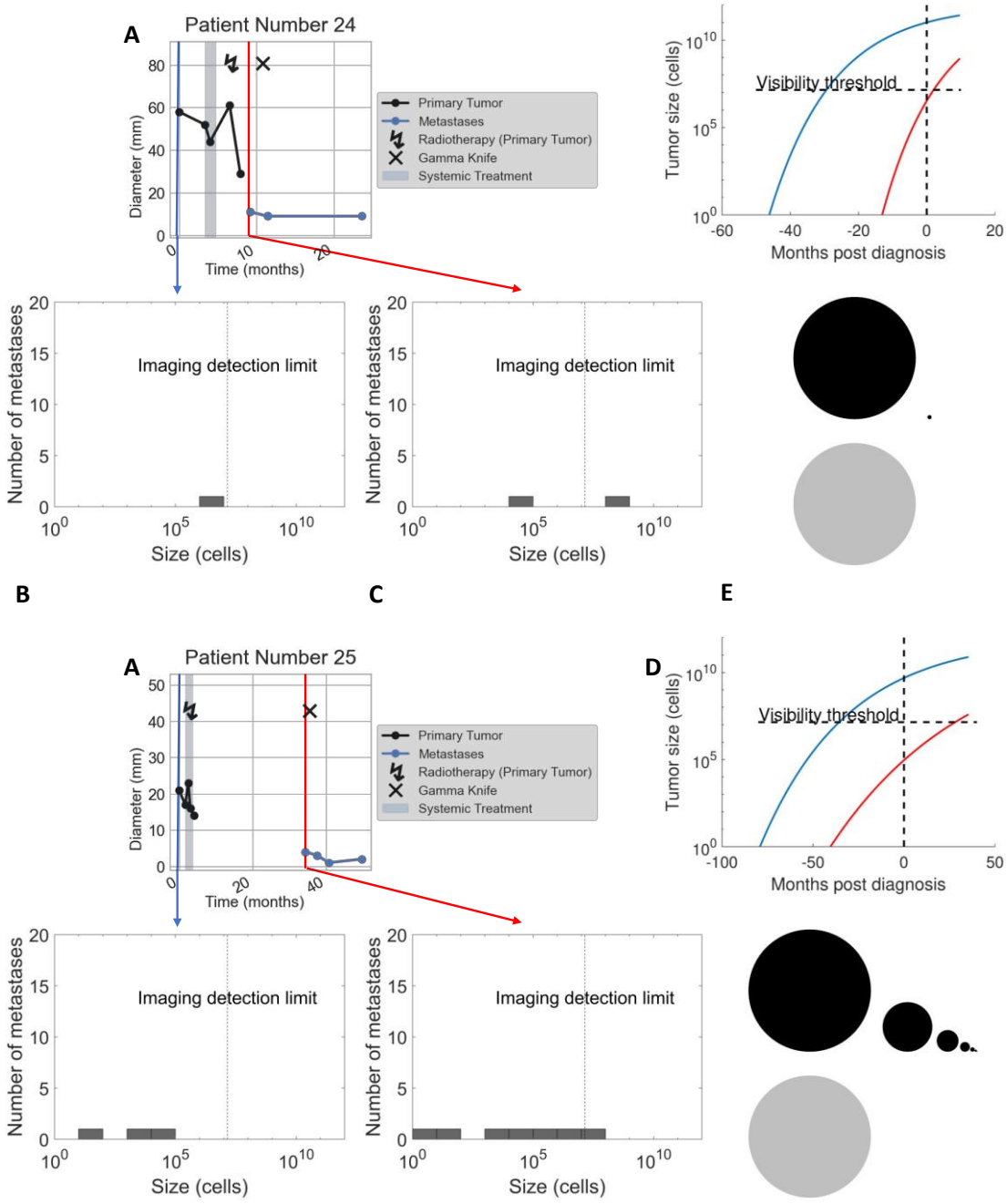
A
Patient Number 24
Diameter (mm)
Time (months)
Primary Tumor
Metastases
Radiotherapy (Primary Tumor)
Gamma Knife
Systemic Treatment
Tumor size (cells)
Visibility threshold
Months post diagnosis
Number of metastases
Imaging detection limit
Size (cells)
B
C
E
A
Patient Number 25
Diameter (mm)
Time (months)
Primary Tumor
Metastases
Radiotherapy (Primary Tumor)
Gamma Knife
Systemic Treatment
D
Tumor size (cells)
Visibility threshold
Months post diagnosis
Number of metastases
Imaging detection limit
Size (cells)

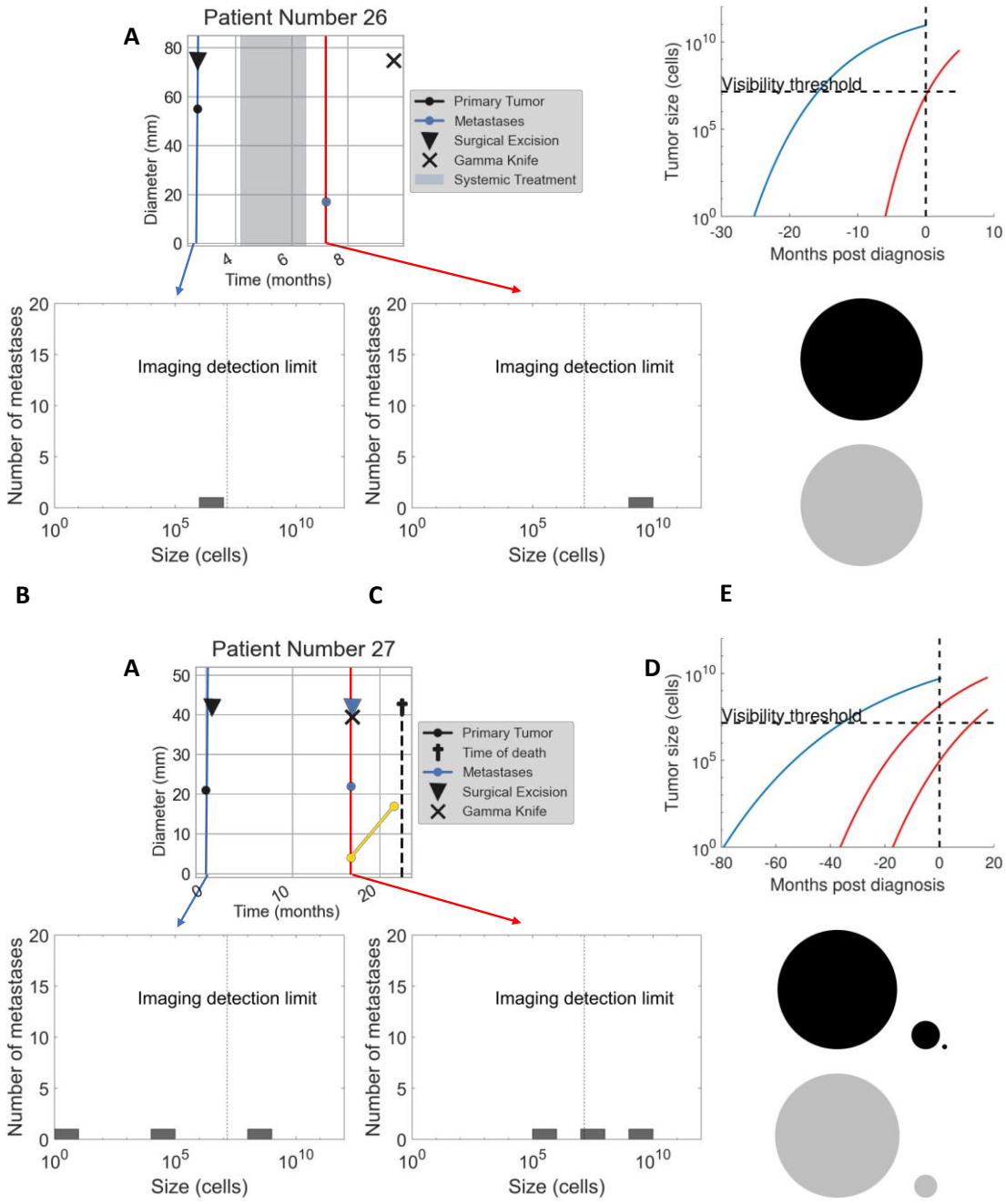
A
Patient Number 26
Diameter (mm)
Time (months)
Primary Tumor
Metastases
Surgical Excision
Gamma Knife
Systemic Treatment
Tumor size (cells)
Visibility threshold
Months post diagnosis
Number of metastases
Imaging detection limit
Size (cells)
B
C
E
A
Patient Number 27
Diameter (mm)
Time (months)
Primary Tumor
Time of death
Metastases
Surgical Excision
Gamma Knife
D
Tumor size (cells)
Visibility threshold
Months post diagnosis
Number of metastases
Imaging detection limit
Size (cells)

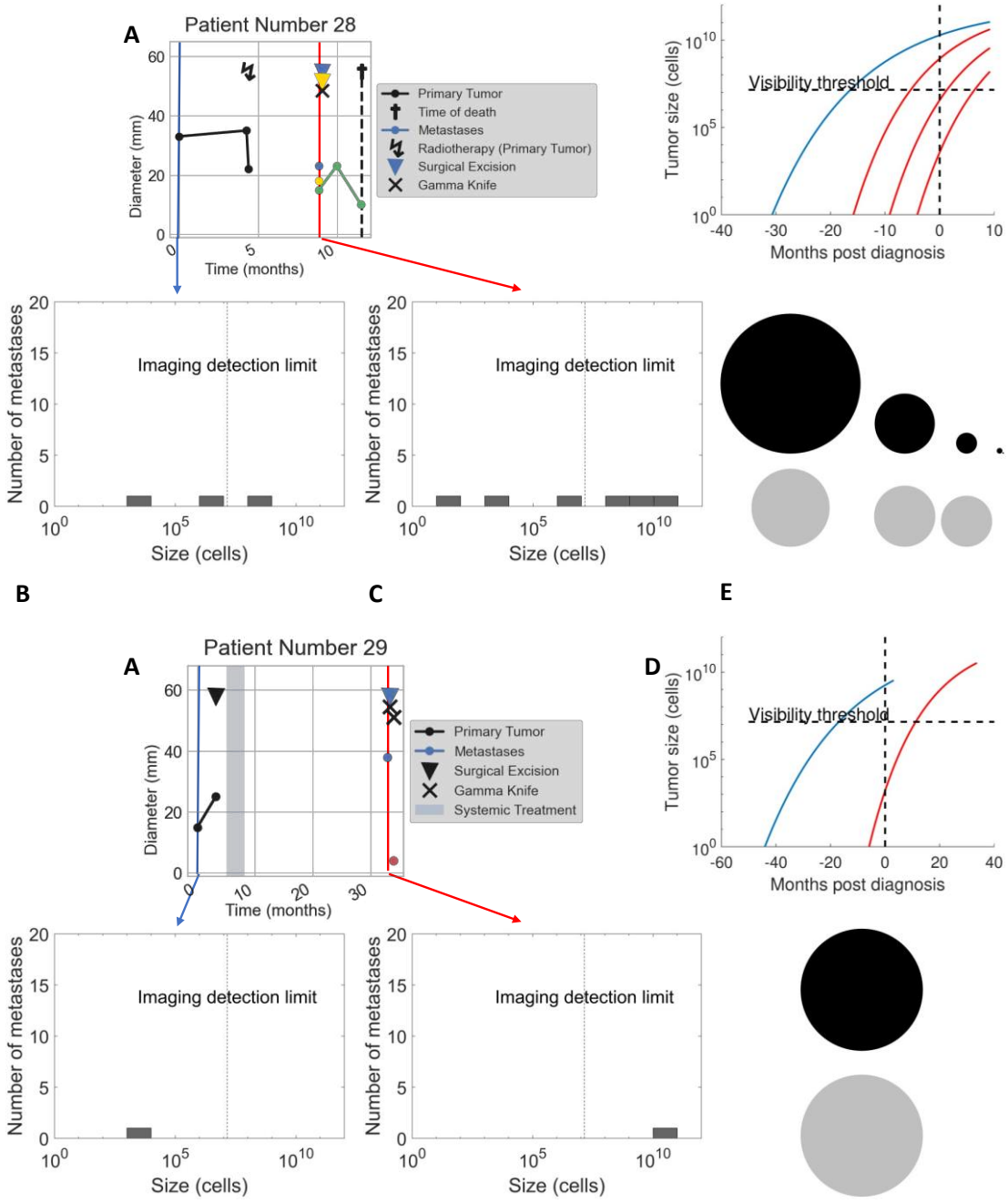
A
Patient Number 28
Diameter (mm)
Time (months)
Primary Tumor
Time of death
Metastases
Radiotherapy (Primary Tumor)
Surgical Excision
Gamma Knife
Tumor size (cells)
Visibility threshold
Months post diagnosis
Number of metastases
Imaging detection limit
Size (cells)
B
C
E
A
Patient Number 29
Diameter (mm)
Time (months)
Primary Tumor
Metastases
Surgical Excision
Gamma Knife
Systemic Treatment
D
Tumor size (cells)
Visibility threshold
Months post diagnosis
Number of metastases
Imaging detection limit
Size (cells)

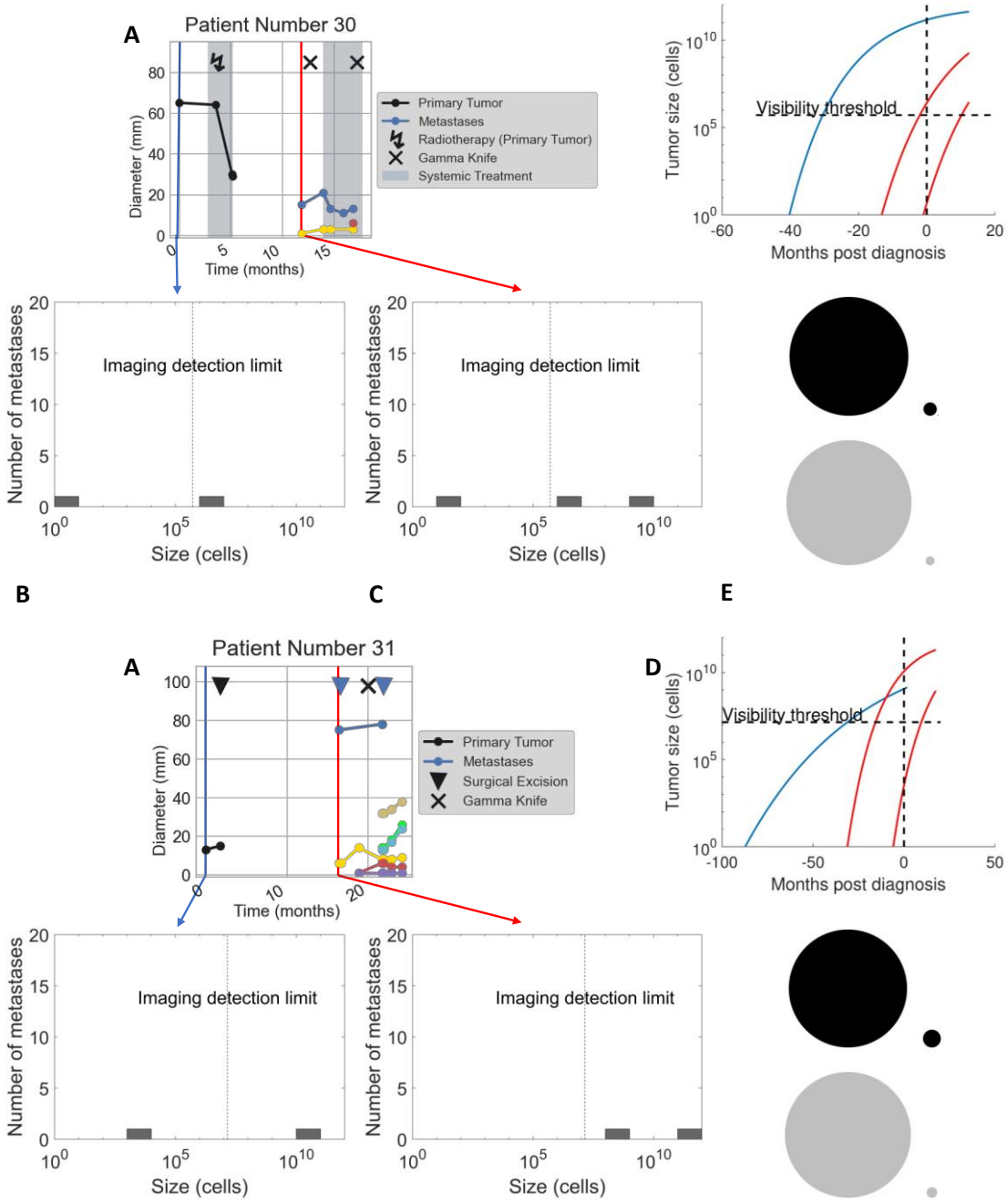
A
Patient Number 30
Diameter (mm)
Time (months)
Primary Tumor
Metastases
Radiotherapy (Primary Tumor)
Gamma Knife
Systemic Treatment
Tumor size (cells)
Visibility threshold
Months post diagnosis
Number of metastases
Imaging detection limit
Size (cells)
B
C
E
A
Patient Number 31
Diameter (mm)
Time (months)
Primary Tumor
Metastases
Surgical Excision
Gamma Knife
D
Tumor size (cells)
Visibility threshold
Months post diagnosis
Number of metastases
Imaging detection limit
Size (cells)